Wiley
International Transactions on Electrical Energy Systems
Volume 2024, Article ID 1074029, 24 pages
https://doi.org/10.1155/2024/1074029

WILEY

Research Article

Investigation of the Impact of SSSC-Based FLC on the Stability of Power Systems Connected to Wind Farms

Ahmadreza Abdollahi Chirani and A. Karami

Faculty of Engineering, University of Guilan, Rasht, Iran

Correspondence should be addressed to Ahmadreza Abdollahi Chirani; bahaminabdollahi@gmail.com

Received 22 November 2023; Revised 11 April 2024; Accepted 14 May 2024; Published 22 May 2024

Academic Editor: Murthy Cherukuri

The integration of renewable energy sources into power systems has increased significantly in recent years. Among various types of renewable energy, the use of wind energy is growing rapidly due to its low operating cost, wide distribution worldwide, and no greenhouse gas emissions. However, power systems integrated with wind energy may face stability and reliability issues due to the intermittent nature of wind power. Therefore, in power systems connected to wind farms, it is usually required to use some compensators such as static synchronous series compensator (SSSC) to increase the system performance under abnormal conditions. On the other hand, for an SSSC to be effective in improving the system performance, it must be equipped with a suitable controller. In this paper, a fuzzy logic controller (FLC) is used for the SSSC because of its advantages over conventional controllers. Extensive research has been conducted in power systems with wind turbines in which SSSC or FLC has been used; however, their simultaneous application in such systems has received less attention. Therefore, this article aims to fill this gap. The proposed method is implemented on two power systems and the simulation results are analyzed. In both systems, the dynamic behavior of three different wind farms is examined. In the first and second wind farms, either a squirrel cage induction generator (SCIG) or doubly-fed induction generator (DFIG) are used, whereas in the third one which is a combined wind farm (CWF), an equal number of SCIG and DFIG are employed. In wind farms with SCIG or DFIG, an SSSC is also utilized. Furthermore, an FLC is employed for the SSSC to improve its efficacy. A proportional integral (PI) controller is also considered for the SSSC, and its results are compared with FLC results. The simulation results confirm the superiority of FLC over PI controller.

1. Introduction

Due to some issues such as environmental pollution, concerns about the consumption of fossil fuel resources, and the reduction of energy costs, significant efforts have been made to develop clean and renewable energy resources such as wind power over the last three decades [1, 2]. It is expected that in the future, renewable energies such as wind and sun will provide a significant amount of electrical energy for the consumers [3, 4]. As a clean and carbon-free renewable energy, wind is one of the most important energy sources on earth. In fact, in addition to lower maintenance and running costs, wind farms need less installation space [5]. However, recent studies have shown that as the penetration levels of wind power plants (WPPs) in power grids increase, problems related to stability and reliability also increase [6, 7]. This is due to the intermittent nature and uncertainty in wind power, which can lead to many challenges in power systems including power quality issues, voltage regulation, and frequency stability [8].

Consequently, it is necessary to develop advanced control strategies and compensation methods in order to keep the balance between supply and demand as well as accommodate unpredictable fluctuations in the WPPs. To achieve this goal, the use of flexible AC transmission system (FACTS) devices has attracted the attention of many researchers [9]. Note that FACTS devices can also be used for other purposes in power systems such as voltage regulation, power loss reduction, and stability improvement [10]. The impact of static synchronous compensator (STATCOM)

and static VAR compensator (SVC) on the voltage stability at the point of common connection (PCC) of a doubly-fed induction generator- (DFIG-) based wind farm, for both the steady-state condition and grid fault condition, has been compared in [11]. The IEEE 9-bus test system was used to assess the effect of FACTS devices on the stability of the network. The WPP was composed of ten individual 5 MW DFIG-based wind turbines. In comparison to SVC, STATCOM was able to provide more reactive power and faster voltage recovery under the same compensation role and capacity. The SVC required a much higher installation capacity than the STATCOM to achieve the same effect.

A TCSC together with a STATCOM was used in [12] to enhance the voltage stability in wind farms. The proposed method can ensure the continuity of power transfer and maintain the voltage stability of the system when the fault occurs. Harmonics in load current were removed with the use of STATCOM control systems, which were employed to improve power quality in the electrical grid. However, one of the main drawbacks of that paper is that it ignores the cost of simultaneous installation of STATCOM and TCSC. In addition, it does not consider oscillations in the active and reactive powers as well. In [13], a wind generator was added to a standard 5-bus network, and the effect of wind energy integration on the voltage stability of the system was investigated. An SVC was also utilized to provide the required injected reactive power for bus voltage regulation. The obtained results showed that SVC can have a significant effect on power flow, voltage regulation, and also power losses in transmission lines. However, the effectiveness of the method proposed in [13] has not been investigated under fault conditions in the power system.

In [14], a STATCOM has been used to effectively control the stability of a multi-machine power system connected to a wind farm. A proportional-integral-derivative (PID) damping controller, a PID with fuzzy logic controller (FLC), and an adaptive neuro-fuzzy inference system (ANFIS) controller were employed for the STATCOM to provide adequate damping for the important modes of the studied system in different operating conditions. Then, it was shown that STATCOM with the proposed ANFIS, STATCOM with PID, as well as STATCOM with both PID and FLC are equally effective in improving system stability.

The performance of SVC and TCSC controllers for the enhancement of small signal stability margin of power systems integrated with intermittent wind power generations has been compared in [15]. It has been concluded that a combination of SVC or TCSC, with a power system stabilizer (PSS), can improve damping of the power system oscillations. It is worth mentioning that PSS increases the complexity of the governing equations of a power system; therefore, in order to improve the performance of power systems with PSS, PSS parameters should be carefully tuned. It can be a challenging task to determine the optimal parameters of a PSS. Furthermore, improper tuning of the PSS parameters may lead to system instability or inadequate damping for the system oscillations.

The performance of a STATCOM connected to a DFIG-based wind farm has been examined in [16]. A proportional-integral (PI) controller and a FLC were used to improve the effectiveness of the employed STATCOM. The STATCOM with FLC was shown to be superior in comparison to STATCOM with PI controller for improving system stability and power quality. However, it is not clear whether Mamdani or Sugeno types of fuzzy controller has been used in [16], since only information regarding the fuzzy membership functions can be found in that paper. In [17], the effect of PSS and static synchronous series compensator (SSSC) on the stability of the IEEE 14-bus test system integrated with a DFIG-based wind farm, has been discussed. The obtained results show that a combination of SSSC and PSS can effectively damp out power system oscillations and improves both the system transient stability and small-signal stability.

The impact of an SSSC on the stability of a hybrid wind farm consisting of a DFIG and a permanent magnet generator (PMG), has been investigated in [18]. To boost the performance of the SSSC, an ANFIS controller has been employed for the SSSC. The proposed ANFIS uses rotor speed variations of the DFIG and PMG as the inputs, and provides the required injected voltage of the SSSC at its output. The results obtained demonstrate that the proposed controller is able to mitigate power system oscillations. In [19], transient stability improvement of a network connected to an SSSC has been presented. An ANFIS controller has been used for the SSSC to improve its performance. Rotor speed deviation and rotor acceleration were utilized as the inputs for the ANFIS controller, and the SSSC-injected voltage was provided at the output of the ANFIS controller. The obtained simulation results showed that the proposed strategy effectively reduces grid oscillations and significantly improves the voltage profile in the studied system. However, the weakness of the proposed method is that the interpretability of ANFIS models decreases as the number of inputs increases. As a result, it could be difficult to understand and explain the behavior of the proposed SSSC controller for complex scenarios. Furthermore, the usefulness of the ANFIS controller depends on the quality and representativeness of the training data used for this controller. The main problem is that it is difficult to obtain accurate and comprehensive training data for practical power system scenarios.

Extensive research has been conducted in power systems with wind turbines in which SSSC or FLC has been used; however, their simultaneous application in such systems has received less attention. Therefore, this paper aims to bridge this gap in the literature by examining the impact of an SSSC-based FLC on the stability of grid-connected wind farms, thereby contributing to the advancement of sustainable and reliable energy infrastructure. In addition, for the SSSC to be effective in improving the system performance, it has been equipped with an FLC in this paper. The FLC allows to develop intelligent controllers that can respond quickly to the system changes, making it a promising approach for handling the challenges of wind power integration.

This article examines the performance of three types of grid-connected wind farms under different fault conditions.

The employed wind farms include a squirrel cage induction generator- (SCIG-) based wind farm, a DFIG-based wind farm, and a combined wind farm (CWF). The CWF consists of an equal number of SCIG and DFIG generators. In the wind farms based on SCIG and DFIG, an SSSC-based FLC has also been used to enhance the behavior of the systems. However, no SSSC is used in the CWF. The proposed approach is implemented on two power systems and the results obtained are analyzed. The first system is a simple system that includes a 9 MW wind farm connected to the grid, and the second system is the IEEE 9-bus test system integrated with a 45 MW wind farm. All simulations are carried out in MATLAB/Simulink software.

To evaluate the effectiveness of the proposed approach, the time variation of wind farms terminal voltage, active power, and reactive power, as well as a system voltage stability index (VSI), are monitored in the event of faults in the studied systems. Furthermore, a PI controller is also used for the SSSC and the obtained results are compared with the results from the FLC. The simulation results obtained show that the proposed method is able to improve the performance of the test systems under various fault conditions.

The main contributions of the present paper are as follows:

(i) The performance of DFIG and SCIG wind farms equipped with SSSC, and CWF without SSSC has been investigated in a simple power system and in the IEEE 9-bus test system.

(ii) Instead of a conventional PI controller, an FLC has been used for the DC voltage regulator of SSSC to improve its behavior.

(iii) A comparative analysis of the proposed SSSC-based FLC and conventional PI controller for different types of faults has been presented and discussed.

The remainder of the paper is organized as follows. Section 2 outlines the structure and modeling of both the SCIG-based wind turbine and the DFIG-based wind turbine. Section 3 describes briefly the configuration of the SSSC. Section 4 represents the FLC and the model of SSSC-based FLC. Section 5 discusses the VSI, which measures the voltage stability of test systems. The test systems used in this study are demonstrated in detail in Section 6, along with the obtained simulation results. The discussion is represented in Section 7. The findings of this research are presented in Section 8.

2. Wind Turbines

In this section, the mathematical modeling of the SCIG and DFIG wind turbines is presented.

2.1. Squirrel Cage Induction Generators. Until recently, squirrel cage induction generators were the most common type of generator due to their simplicity of construction, high efficiency, and low maintenance requirements [20]. Figure 1 shows an SCIG connected to the network. The SCIGs are directly connected to the system and often operate at a constant speed; therefore, they are sometimes called constant speed wind turbines. The SCIG needs to absorb reactive power from the system and this slows down the process of voltage restoration when a fault occurs in the system [21]. As a result, the system may experience some oscillations in the voltage and rotor speed. Moreover, the unbalance between mechanical power drawn from the wind and electrical power transmitted to the network makes the generator to accelerate during the fault conditions. If the generator voltage is not restored in the postfault state, the generator will continue to consume more reactive power from the system. Voltage and rotor-speed instability could eventually result from this process, which is highly possible if the wind turbine is connected to a weak network [22]. The following equation gives the mechanical power drawn from the wind by the rotor of the SCIG and the DFIG wind turbines [23, 24]:

$$P_{\text{Wind}} = \frac{1}{2}\rho\pi r^2 v^3 C_p(\beta,\lambda), \tag{1}$$

where C_P is the performance coefficient of wind turbine which expresses the rotor efficiency of the turbine (extracted power/wind power), ρ is the air density (kg/m^3) r is the turbine radius (m), V is the wind velocity (m/s), and P_{Wind} is the wind power (W). The electromagnetic torque T_e can be written as follows [25, 26]:

$$T_e = L_m\left(i_{sd}i_{rq} - i_{sq}i_{rd}\right). \tag{2}$$

The relations between the mechanical torque and angular speed of the rotor can be described as follows [27, 28]:

$$\begin{aligned} 2H_m\frac{d\omega_m}{dt} &= T_m - K_s\theta_s,\\ 2H_G\frac{d\omega_G}{dt} &= K_s\theta_s - T_e,\\ \frac{d\theta_s}{dt} &= \omega_B - (\omega_M - \omega_G), \end{aligned} \tag{3}$$

where H_m and H_G are the inertia constants of wind turbine rotor and generator rotor, respectively; ω_M is wind turbine speed and ω_G is generator speed, K_s is the stiffness coefficient of the axis, and θ_s is the rotation angle of the rotor axis [29].

Equation (4) is used for mathematical modeling of the SCIG [29]:

$$\begin{bmatrix} v_{qs}\\ v_{ds}\\ 0\\ 0 \end{bmatrix} = \begin{bmatrix} r_s + pl_s & 0 & pl_{ms} & 0\\ 0 & r_s + pl_s & 0 & pl_{ms}\\ pl_{ms} & -\omega_r l_{ms} & r'_r + pl'_r & -\omega_r l'_r\\ \omega_r l_{ms} & pl_{ms} & \omega_r l'_r & r'_r + pl'_r \end{bmatrix} \begin{bmatrix} i_{qs}\\ i_{ds}\\ i'_{qr}\\ i'_{dr} \end{bmatrix}, \tag{4}$$

where r'_r and r_s are the rotor and stator resistances, i_{ds} and i_{qs} are the stator currents transferred to the direct and quadrature axes, i'_{dr} and i'_{qr} are the rotor currents transferred to the d and q axes, V_{ds} and V_{qs} are the stator voltages transferred to the d and q axes, ω_{r} is the rotor shaft mechanical speed, l_{ms} is the stator magnetizing inductance, l'_r is

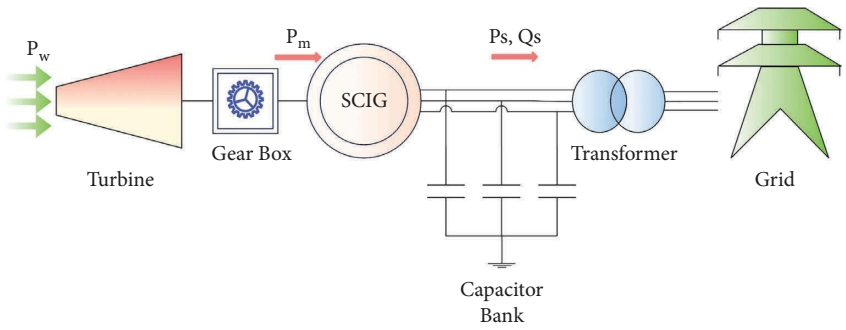

Figure 1: Constant speed wind turbine equipped with squirrel cage induction generator (SCIG).

the rotor inductance, l_s is the stator inductance, and p is the time derivative operator.

In order to prevent surpassing the output power limit of the wind turbine, the stall effect or pitch angle control is used to restrict the wind input mechanical power. In fact, the rotor is designed to reduce its aerodynamic efficiency as the wind speed increases to avoid drawing too much mechanical power from the wind. The active and reactive powers of the stator can be calculated as follows [30]:

$$P_s = \left(\frac{3}{2}\right)\left(V_{ds}I_{ds} + V_{qs}I_{qs}\right),$$
$$Q_s = \left(\frac{3}{2}\right)\left(V_{qs}I_{ds} - V_{ds}I_{qs}\right). \quad (5)$$

2.2. Doubly-Fed Induction Generator. Doubly-fed induction generator (DGIG) wind turbines are based on wound-rotor induction machines where the rotor circuit is fed through bidirectional back-to-back voltage source converters [31]. A schematic model of the DFIG is shown in Figure 2. The DFIG is the most commonly used wind turbine for wind power generation, since it provides significant benefits such as variable speed, high-power output, decoupled control of active and reactive powers, and power quality improvement [32, 33]. As shown in Figure 2, the rotor winding of a DFIG is connected to a converter through slip rings, whereas its stator winding is directly connected to the network. The electric power of the converter is about 20 to 30% of the total electric power of the generator [34].

The back-to-back voltage converter via the DC link capacitor feeds rotor from the third winding of a three-winding transformer that connects the DFIG to the network [33]. Power is transferred from the stator to the network through two of three windings of the three-winding transformer. The DFIG allows wind turbines to generate maximum power and can maintain grid voltage stability by regulating the reactive power transfer, regardless of the wind speed. The converter near the rotor is known as the rotor side converter (RSC), and the converter near the grid is known as the grid side converter (GSC). The purpose of RSC is to regulate both the active and reactive powers, and GSC adjusts the power factor and voltage of the coupling capacitor [35, 36].

The following equation is used for mathematical modeling of the DFIG [27]:

$$\begin{bmatrix} v_{qs} \\ v_{ds} \\ v'_{qr} \\ v'_{0r} \end{bmatrix} = \begin{bmatrix} r_s + pl_s & 0 & pl_{ms}\cos\theta_r & -pl_{ms}\sin\theta_r \\ 0 & r_s + pl_s & pl_{ms}\sin\theta_r & pl_{ms}\cos\theta_r \\ pl_{ms}\cos\theta_r & pl_{ms}\sin\theta_r & r'_r + pl'_r & 0 \\ -pl_{ms}\sin\theta_r & pl_{ms}\sin\theta_r & 0 & r'_r + pl'_r \end{bmatrix} \begin{bmatrix} i_{qs} \\ i_{ds} \\ i'_{qr} \\ i'_{dr} \end{bmatrix}. \quad (6)$$

The rotor active power and reactive power are calculated by the following equations [29]:

$$P_r = \left(\frac{3}{2}\right)\left(V_{dr}I_{dr} + V_{qr}I_{qr}\right),$$
$$Q_r = \left(\frac{3}{2}\right)\left(V_{qr}I_{dr} - V_{dr}I_{qr}\right). \quad (7)$$

The mechanical power and stator electrical power output of the DFIG are as follows [37]:

$$P_m = T_m\omega_r,$$
$$P_s = T_{em}\omega_s, \quad (8)$$

where T_m represents the rotor mechanical torque, ω_r represents the rotor speed, T_{em} is the electromagnetic torque, and ω_s is the synchronous speed.

3. Static Synchronous Series Compensator

The static synchronous series compensator is a voltage source converter- (VSC-) based FACTS device that was developed in 1989 for series compensation [38]. The SSSC is a series FACTS device which can control the flow of power and is able to reduce power oscillations in the network. The SSSC has a significant impact on the power distribution, due to its ability to change the impedance of transmission line

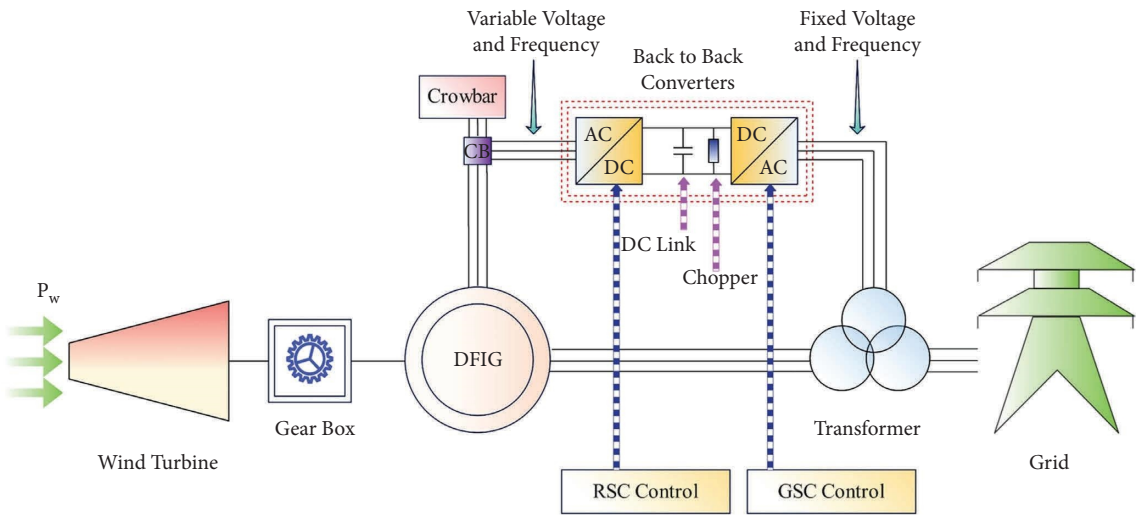

Figure 2: Variable speed wind turbine equipped with doubly-fed induction generator (DFIG).

[39]. In fact, the main objective of an SSSC is to increase the maximum transferable power of the system by reducing the reactance of the transmission line. The schematic model of an SSSC is shown in Figure 3. Here, A and B denote the sending end and receiving end buses, respectively. At the receiving bus B, active and reactive powers are calculated as follows [40]:

$$P = \frac{V_A V_B}{X_L} \sin(\delta_A - \delta_B),$$
$$Q = \frac{V_A V_B}{X_L} (1 - \cos(\delta_A - \delta_B)), \quad (9)$$

where X_L is the inductive reactance of transmission line, V_A and V_B are, respectively, voltage magnitudes at buses A and B. Also, δ_A and δ_B denote phase angles of the voltages at buses A and B, respectively.

The SSSC is synchronized with the transmission line current I and injects a series voltage V_{inj} that is orthogonal to the current, either lagging or leading. Notice that the VSC internal losses need to be compensated by a small amount of active power. The DC capacitor can be kept charged without an external power source by drawing power from the line through a minor deviation from the ideal 90° [17, 41]. The SSSC can be a simple and cost-effective choice for the regulation of both the active power and reactive power in long transmission lines. In fact, it can improve the power transfer capabilities in the transmission line, thereby enhancing power system stability. This is crucial for transmitting power from remote wind farms to urban areas with high power demand, where long transmission lines are often employed. The grid reliability can also be increased by using the SSSC. In addition, the SSSC can prevent improper exploitation of generators and can avoid conditions that may lead to loss of some loads in the network [10].

In wind farms, especially those located far from the load centers, voltage oscillations can occur due to variations in both the wind speed and the wind power. In long transmission lines, the voltage drop is usually high. An SSSC can help maintain voltage levels within acceptable limits by regulating the reactive power. In fact, by reducing the series impedance of the transmission line, an SSSC reduces the electrical length of transmission line and improves the system stability. Figure 4 illustrates the control system of an SSSC. This control system functions as follows [19]:

(i) The output of a phase-locked loop (PLL), which is the phase angle ($\theta = \omega t$), generates components of both the direct-axis voltage and current (V_d and I_d) and the quadrature-axis voltage and current (V_q and I_q) of the AC three-phase system.

(ii) The measurement systems compute the quadrature-axis components of the AC positive-sequence for the voltages V_1 and V_2 as well as for the DC voltage V_{dc}.

(iii) The reference DC voltage (V_{dcref}) and the injected voltage (V_{qref}) are determined by the AC and DC voltage regulators to generate the voltages of converter (V_{dcnv} and V_{qcnv}).

4. Proposed Method

4.1. SSSC-Based Fuzzy Logic Controller. Fuzzy logic controller (FLC) is known as one of the nonlinear and reliable control methods, which is based on expert knowledge. In fact, the FLC does not require an accurate model of the system under study [42]. A well-designed FLC can perform more efficiently than a conventional PI controller in the case of parameters variations, external disturbances, as well as load variations [16]. The benefits of employing FLC over the standard PI controller include its universal control design, simplicity, adaptability, quick response, and insensitivity to the parameter's changes. In addition, it can perform appropriately even with imprecise input signals [43]. On the other hand, parameters tuning of a PI controller is not an easy task. Instead, an FLC does not require an accurate model of the system under study, and it is also robust against system changes. In this paper, the employed fuzzy rules and

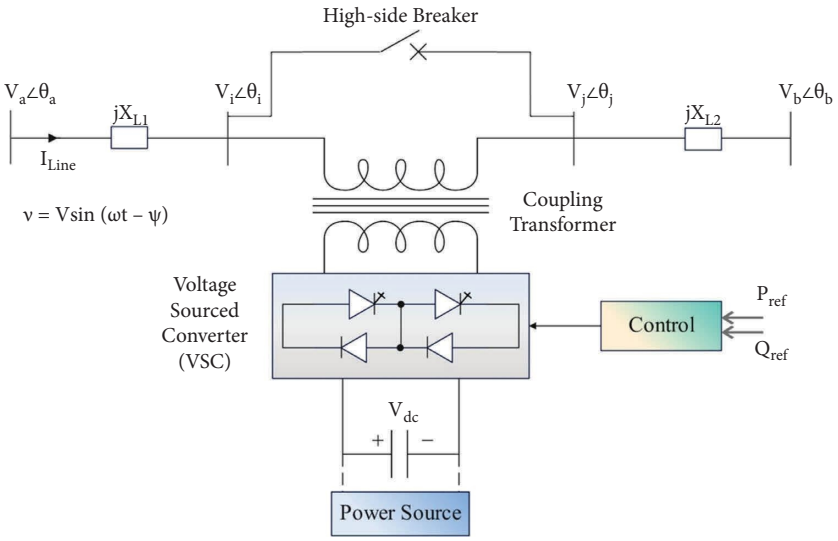

Figure 3: The schematic model of an SSSC.

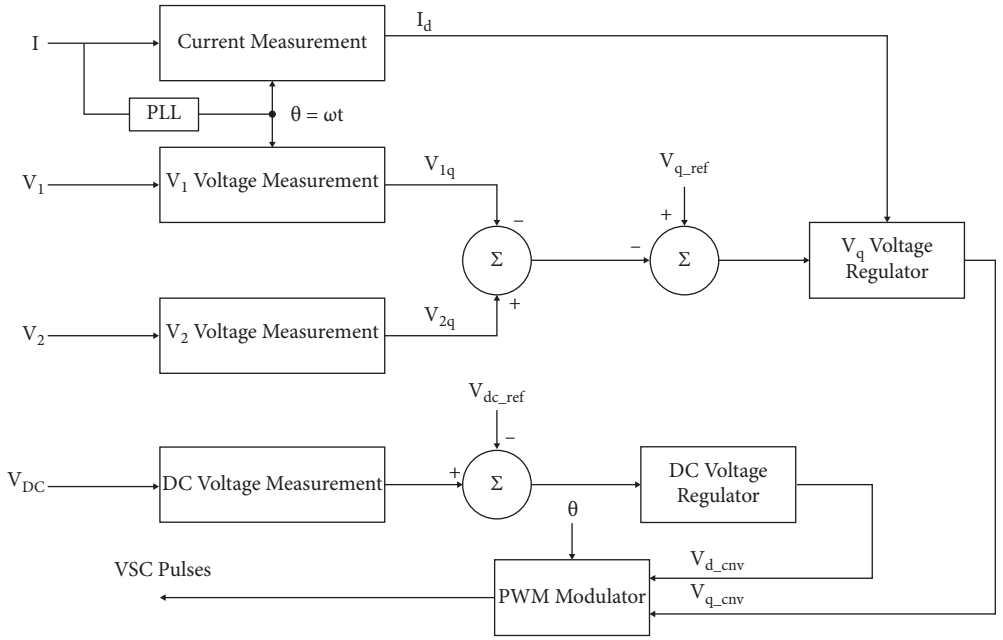

Figure 4: The schematic diagram of the SSSC control system.

the required membership functions have been obtained by using a trial-and-error approach. A general outline of the design process of SSSC-based FLC is given in the following.

4.2. Inputs and Outputs of FLC. The FLCs have some inputs and outputs that need to be determined in the first step. Figure 5 illustrates the proposed fuzzy logic controller-based voltage regulator used for the SSSC. The first input of the FLC is error, which is the difference between the reference DC voltage (V_{dc-ref}) and the actual DC voltage (V_{dc}), (Error = $V_{dc-ref} - V_{dc}$). The second input is the change of error. The FLC output is the direct component of the converter voltage (V_{d-con}).

4.3. Defining Fuzzy Sets. In the second step, the linguistic variables and fuzzy sets must be defined for both inputs and outputs. Linguistic variables show the linguistic terms used to explain the system's behavior. The linguistic variables are considered as follows: (NB) = Negative Big; (NM) = Negative Medium; (NS) = Negative Small; (Z) = Zero; (PS) = Positive Small; (PM) = Positive Medium; (PB) = Positive Big [44, 45].

4.4. Formulation of Fuzzy Rules. The third step is to create a set of fuzzy rules that can capture the control strategy. These rules map combinations of input fuzzy sets to appropriate output fuzzy sets. The rule base should reflect both the control objectives and expert knowledge about the

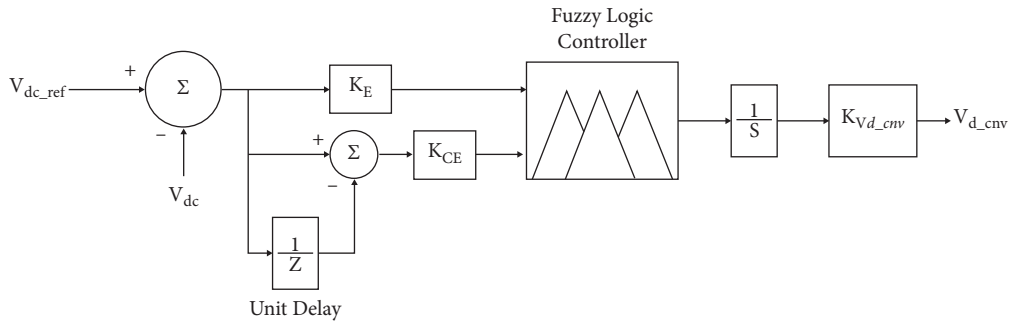

Figure 5: Proposed fuzzy logic controller-based voltage regulator for SSSC.

system. The employed FLC rules are given in Table 1. Note that practical experiences are generally taken into consideration for the development of rules. The following three conditions show how the rule base is developed [46]:

(i) If error is NM and change of error is NS then the output is NB.

(ii) If error is Z and change of error is PB then the output is PB.

(iii) If error is PM and change of error is NM then the output is Z.

4.5. Defining Fuzzy Membership Functions. In the fourth step, the fuzzy membership functions of the inputs and outputs variables are determined. The shape and parameters of these functions determine how input/output values are mapped to the values of membership functions in the fuzzy set. The FLC of this paper consists of two inputs each with 7 linguistics values that generate 49 rules [44, 45]. The inputs and output of the FLC rule base of the proposed fuzzy control-based DC voltage regulator are considered as triangular type, due to the following merits. Triangular membership functions are symmetric in shape, with the peak located at the center of the interval defined by the left and right boundaries. This symmetry reduces the design complexity and gives equal importance to both sides of the peak. It also ensures a symmetrical and balanced system response around the peak value. Furthermore, triangular membership functions require less computation than other membership functions with complex shapes. In addition, the degree of membership for a given input value can be computed more quickly and with fewer computations by using a triangle membership function.

The designed membership functions for the error as the first input, is shown in Figure 6(a). The vertical axis shows the degree of membership, and it ranges between 0 and 1. The horizontal axis represents the error which varies in the range $[-1, 1]$. Figure 6(b) shows the membership functions designed for change of error as the second input. A scale of 0 to 1 indicates the degree of membership on the vertical axis. The horizontal axis shows change of error in the range of $[-1, 1]$. The designed membership functions for V_{d-con} as the output signal, is shown in Figure 6(c). The vertical axis shows the degree of membership and it ranges between 0 and 1. The horizontal axis represents the direct component of the converter voltage, which varies in the range $[-1, 1]$.

Table 1: FLC rules for the proposed controller.

Error (E)	Change of error (CE)						
	NB	NM	NS	Z	PS	PM	PB
NB	NB	NB	NB	NB	NM	NS	Z
NM	NB	NB	NB	NM	NS	Z	PS
NS	NB	NB	NM	NS	Z	PS	PM
Z	NB	NM	NS	Z	PS	PM	PB
PS	NM	NS	Z	PS	PM	PB	PB
PM	NS	Z	PS	PM	PB	PB	PB
PB	PB	PB	PB	PB	PB	PB	PB

4.6. Fuzzy Inference. The fifth step is to apply fuzzy inference to determine the appropriate output fuzzy sets based on the input fuzzy sets and the assumed fuzzy rules. The inference procedure generates a fuzzy output by combining the fuzzy rules with the membership degrees. Several inference algorithms, such as Mamdani and Sugeno, are available for deployment. This research employed Mamdani type FLC instead of Sugeno type FLC due to the following advantages. The Mamdani FLC uses linguistic variables and fuzzy rules that can be easily interpreted by humans. It functions satisfactorily in the presence of uncertainty and insufficient inputs. The inherent uncertainty in real-world systems can be captured and modeled with the use of fuzzy sets and linguistic concepts. Its robustness to uncertainty makes Mamdani FLC suitable for applications in which precise mathematical models are not available or difficult to obtain. Moreover, it can be easily implemented for the control of DC voltage regulator in the SSSC.

4.7. Implementation. In the last step, the PI controller in the DC voltage regulator of the SSSC is replaced by the designed FLC. Then, the performance of the proposed FLC is assessed by performing time-domain simulations. For this purpose, active and reactive powers as well as voltage at the PCC of wind farms are analyzed. In addition, the simulation results obtained from the FLC are compared with the results obtained from a PI controller to verify its effectiveness.

5. Voltage Stability Index

The employed voltage stability index is described in this section. The risk of voltage instability in the electrical grid is estimated by using this index. It should be noted that

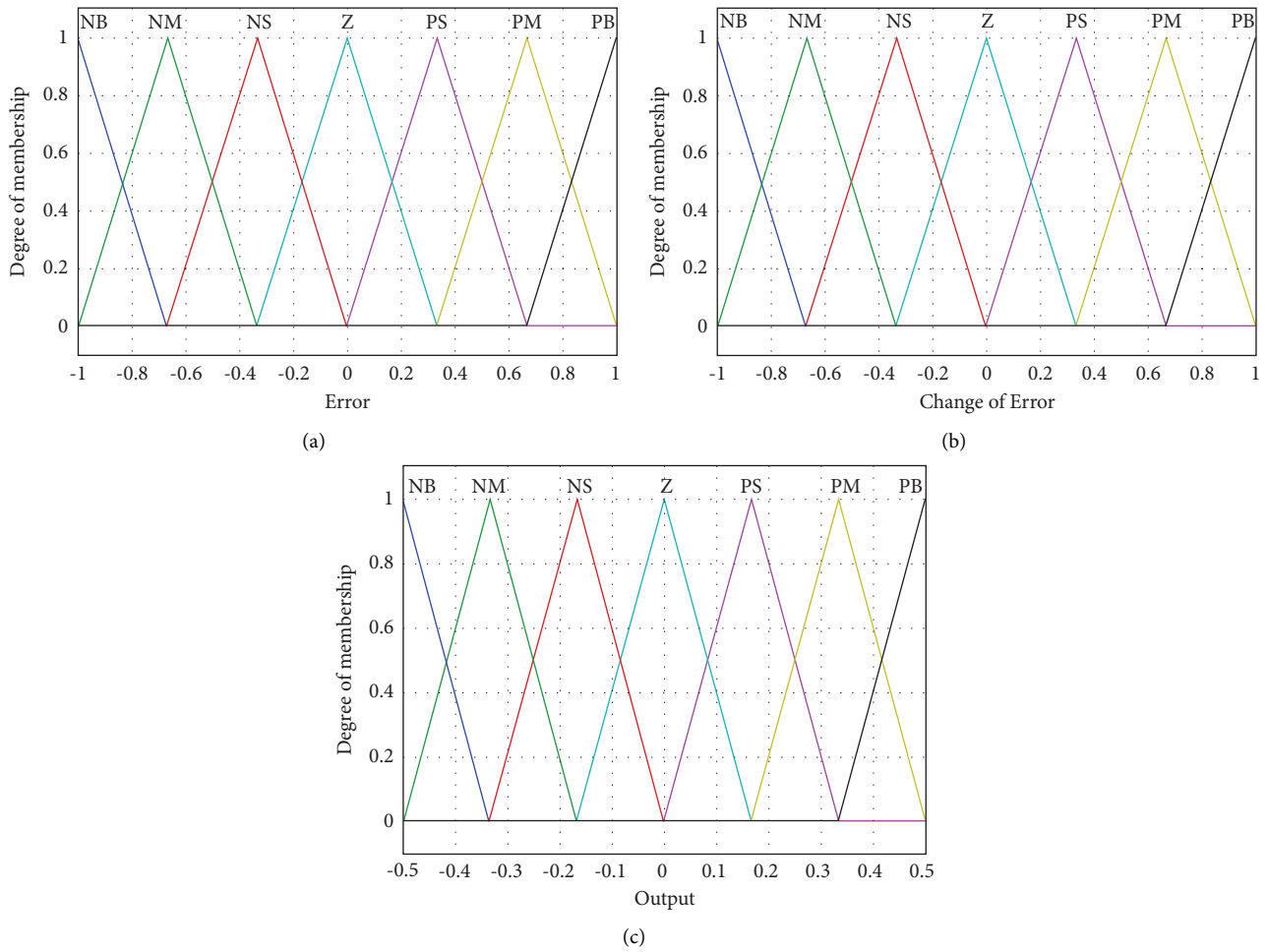

Figure 6: FLC membership functions for: (a) error signal, (b) change of error signal, (c) output signal.

different methods can be used to obtain various voltage stability indices in power systems [47, 48]. The VSI, which was proposed in reference [49], is utilized in the present work to assess the voltage stability of the power systems under study [50]. Consider a transmission line in a multimachine power system, as shown in Figure 7, where usual notations have been adopted. In Figure 7, buses i and j show the sending bus and receiving bus of the transmission line, respectively.

Based on the value obtained for VSI, the following conclusions can be drawn about the system voltage stability:

(i) VSI greater than 1 specifies that the transmission line is in its power transmission range.

(ii) VSI equal to 1 indicates the maximum power transfer capability of the transmission line.

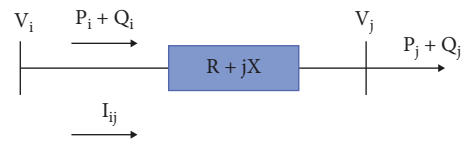

Figure 7: Schematic representation of a two-bus transmission system.

(iii) VSI of less than 1 shows violation in maximum transferable power and thus indicates system voltage instability.

The employed VSI is calculated by using the following equation [49]:

$$\mathrm{VSI} = \frac{|V_i|^2\sqrt{\left[\left(P_i - |I|^2R\right)^2 + \left(Q_i - |I|^2X\right)^2\right]\left(R^2 + X^2\right)}}{2\left(P_iX - Q_iR\right)^2} - \frac{|V_i|^2\left[\left(P_i - |I|^2R\right)R + \left(Q_i - |I|^2X\right)X\right]}{2\left(P_iX - Q_iR\right)^2}, \tag{10}$$

where V_i is the voltage at bus i, P_i is the load active power at bus i, Q_i is the load reactive power at bus i, I is the transmission line current. Also, R and X are the resistance and reactance of transmission line, respectively.

6. Test Systems and Simulation Results

The proposed method is implemented on two power systems. The first system is a simple system that includes a 9 MW wind farm connected to a grid, and the second system is the IEEE 9-bus test system integrated with a 45 MW wind farm. In both systems, three types of wind farms have been utilized. In the first system, three different combinations of wind farms have been used. Therefore, a total of 4 test systems (known here as Systems A, B, C, and D), were considered. As shown in Figure 8, in System A there are six 1.5 MW DFIG-based wind turbines with a total output of 9 MW. System B, which is shown in Figure 9, consists of six 1.5 MW SCIG-based wind turbines with a total output of 9 MW. The general scheme of System C that includes a combined wind farm (CWF), is illustrated in Figure 10. The CWF is composed of three 1.5 MW SCIG wind turbines and three 1.5 MW DFIG wind turbines for a total output of 9 MW. In system D, which is indeed the modified IEEE 9-bus system, SCIG wind farm, DFIG wind farm, as well as CWF are used.

In Systems A and B, the wind farms are represented by three sets each with two wind turbines. Each set of wind turbine is connected to a 25 kV/575 V transformer and is located at a distance of 1 km from the PCC (i.e., bus B1). In each set of SCIG wind turbine, a 400 kVAr capacitor bank is also used. Moreover, a 500 kW load is connected to each set of DFIG wind turbine. The voltage at bus B1 is equal to 25 kV. The wind speed was assumed to be 10 m/s. The wind farms are connected to a 25 kV distribution system and transmit power to a 120 kV grid through a 25 km and 25 kV feeder. In both Systems A and B, the wind farms are equipped with an SSSC near bus B1, as shown in Figures 8 and 9. As can be seen in Figure 10, there is no SSSC connected to System C; however, a 400 kVAr capacitor bank and a 500-kW load are connected to the SCIG and DFIG-based wind turbines, respectively. Again, the wind speed is assumed to be 10 m/s. The parameters of the SCIG, DFIG, and SSSC of the test systems, are provided in the Appendix.

For Systems A, B, and C, the behavior of the employed wind farms under both single-phase fault and three-phase fault conditions was examined. The faults are assumed to occur at bus B2 at 15 s from the start of simulation, and are cleared at 15.2 s (i.e., faults are cleared in 0.2 s). The simulation results obtained for terminal voltage, active power, and reactive power at the PCC are presented.

In System D, which is widely used for power systems stability study, the synchronous machines are equipped with voltage regulators combined with an exciter and comprehensive model of steam turbine and governors. All loads are modeled using three-phase parallel RLC PQ load blocks (Y grounded configuration). An IEEE type 1 excitation system is used for all voltage regulators. The data for System D (i.e., IEEE-9 bus system) can be found in [51].

In Figure 11, the wind farms are connected to bus B5, and the faults are also assumed to occur at bus B5. There are thirty 1.5 MW wind turbines in the DFIG and SCIG wind farms, which result in a total output of 45 MW. However, the CWF is composed of fifteen 1.5 MW SCIG wind turbines and fifteen 1.5 MW DFIG wind turbines for a total output of 45 MW. Each wind farm is connected to a 25 kV/575 V transformer and is located at a distance of 10 km from the PCC. In the DFIG-based wind turbines and SCIG-based wind turbines, the wind farms are equipped with an SSSC. However, there is no SSSC connected to the CWF of System D, as shown in Figure 11. The performance of the employed wind farms under both three-phase fault and line-to-line fault was studied in System D. The simulation results obtained for terminal voltage, active power, and reactive power at the PCC (i.e., bus B5) are presented. Note that although all the three wind farms are shown in Figure 11, in each simulation, it is assumed that only one wind farm, i.e., one of the SCIG, DGIG, or CWF, is connected to the IEEE 9-bus system.

6.1. Simulation Results for Single-Phase Fault on Systems A, B, and C

6.1.1. Active Power Variation. In this section, it is assumed that a single-phase to ground fault of 0.2 seconds duration occurs at bus B2 in Systems A, B, and C. As shown in Figure 12, active power of the DFIG wind farm decreases to 8.1 MW during the faulted period; however, it quickly recovers to its prefault value in the postfault state. Nevertheless, it can be seen that with the presence of SSSC in the DFIG wind farm, the conventional (PI) controller and FLC have almost the same effect on the active power oscillations. It can also be seen that in the postfault period, thanks to the presence of SSSC, oscillations in the active power of the DFIG wind farm are less than the corresponding oscillations in the CWF without the SSSC. During the faulted period, the active power level of the SCIG wind farm, either with SSSC-based FLC or with SSSC-based PI controller, is higher than that of DFIG wind farm.

The output power of the SCIG wind farm, which is equal to 8.95 MW in the prefault state, decreases to 8.93 MW during the faulted period, that is, this wind farm experiences only a 0.02 MW reduction in its output power. As illustrated in Figure 12, in the faulted period, CWF- and DFIG-based wind farm experience, respectively, 0.71 MW and 0.79 MW reductions in their active powers. Therefore, regarding active power variation and for the case of single-phase fault, the SCIG wind farm with an SSSC has shown superior performance, compared to the CWF and DFIG wind farm. This superiority is due to the fact that in the case of single-phase to ground faults, the SCIGs are still capable of generating electrical power during the faulted period.

6.1.2. Terminal Voltage Variation. Figure 13 shows the terminal voltage variation at the PCC of wind farms for a 0.2 seconds duration single-phase to ground fault at bus B2 in Systems A, B, and C. As can be seen in Figure 13, terminal

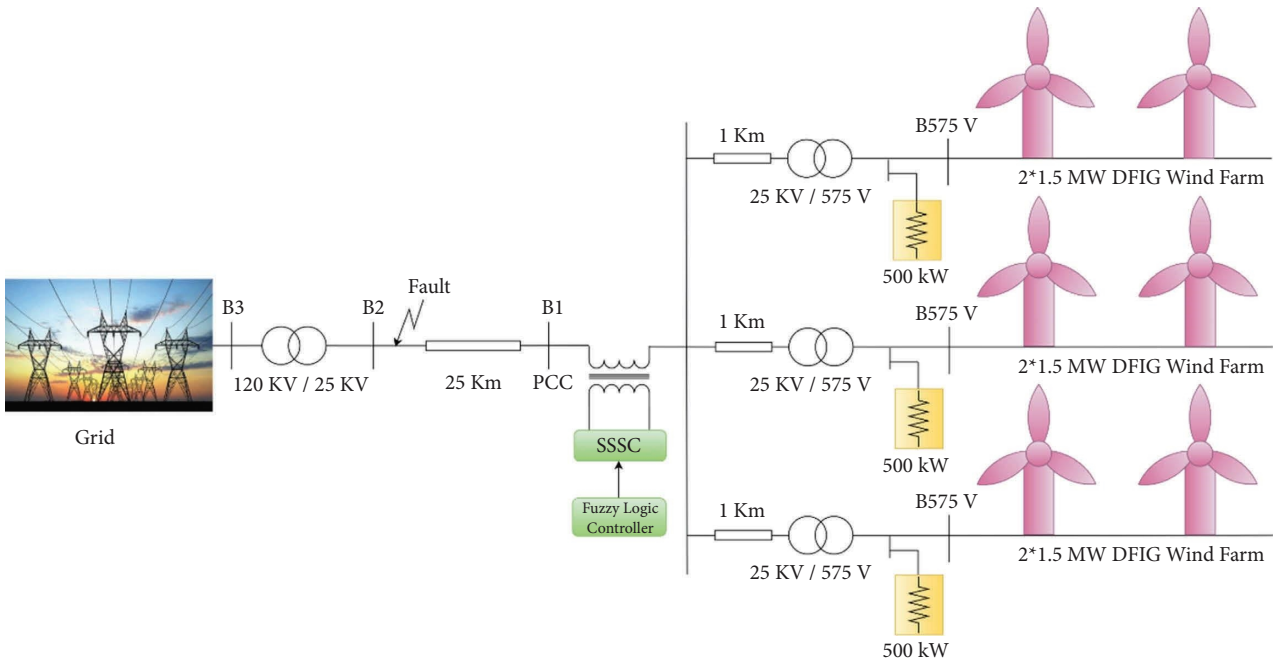

Figure 8: Schematic diagram of wind farm based on DFIG (System A).

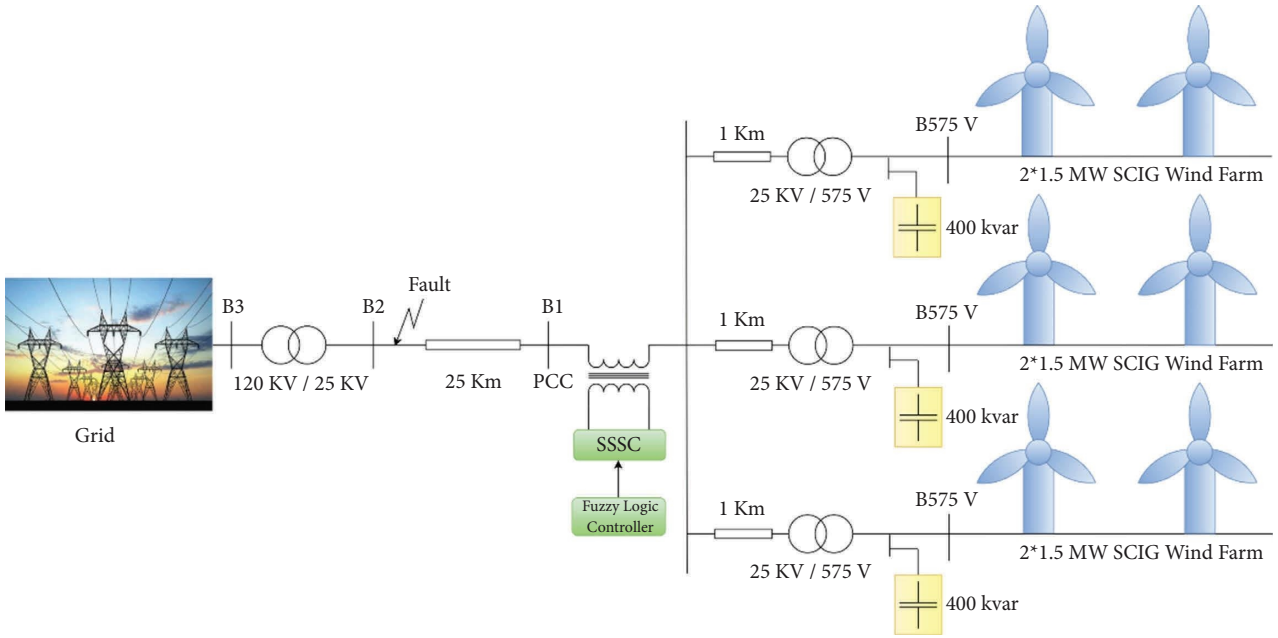

Figure 9: Schematic diagram of wind farm based on SCIG (System B).

voltage in all the employed wind farms decreases drastically during the faulted period. However, voltages of all the wind farms return back, very quickly and without any oscillations, to their prefault values in the postfault state. Therefore, we can conclude that regarding terminal voltage variation and in the event of single-phase fault, all the employed wind farms have performed similarly.

6.1.3. Reactive Power Variation. The variation in reactive power of wind farms for a 0.2 seconds duration single-phase fault at bus B2 in Systems A, B, and C, is shown in Figure 14. As can be seen in this figure, all the wind farm experience only a little variation in their absorbed reactive powers, in the faulted period. Furthermore, we can observe that the DFIG farm with the SSSC-based PI controller absorbs the

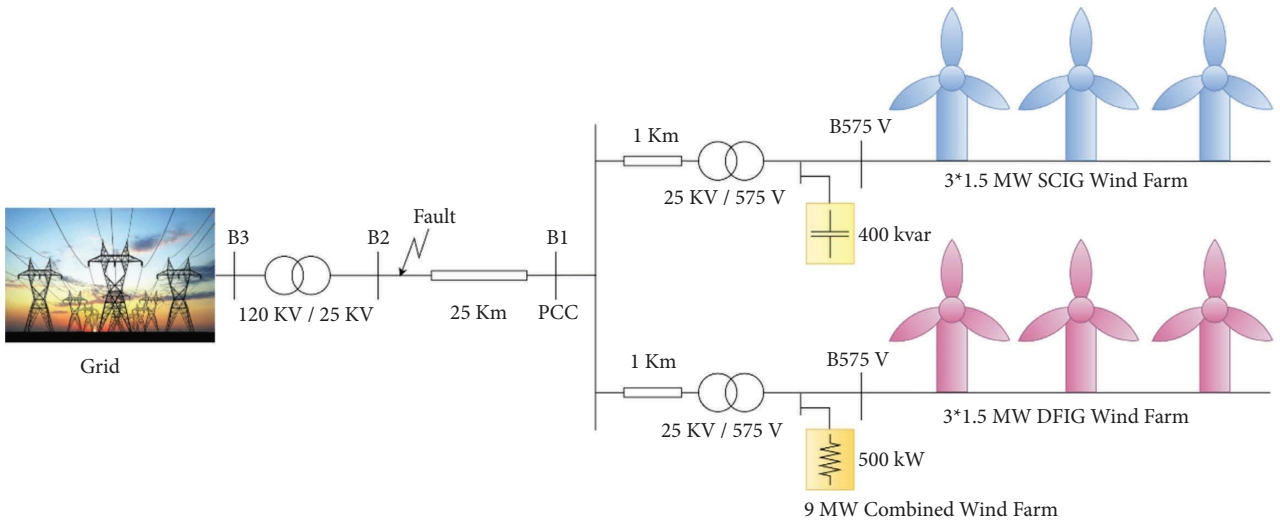

Figure 10: Schematic diagram of CWF without SSSC (System C).

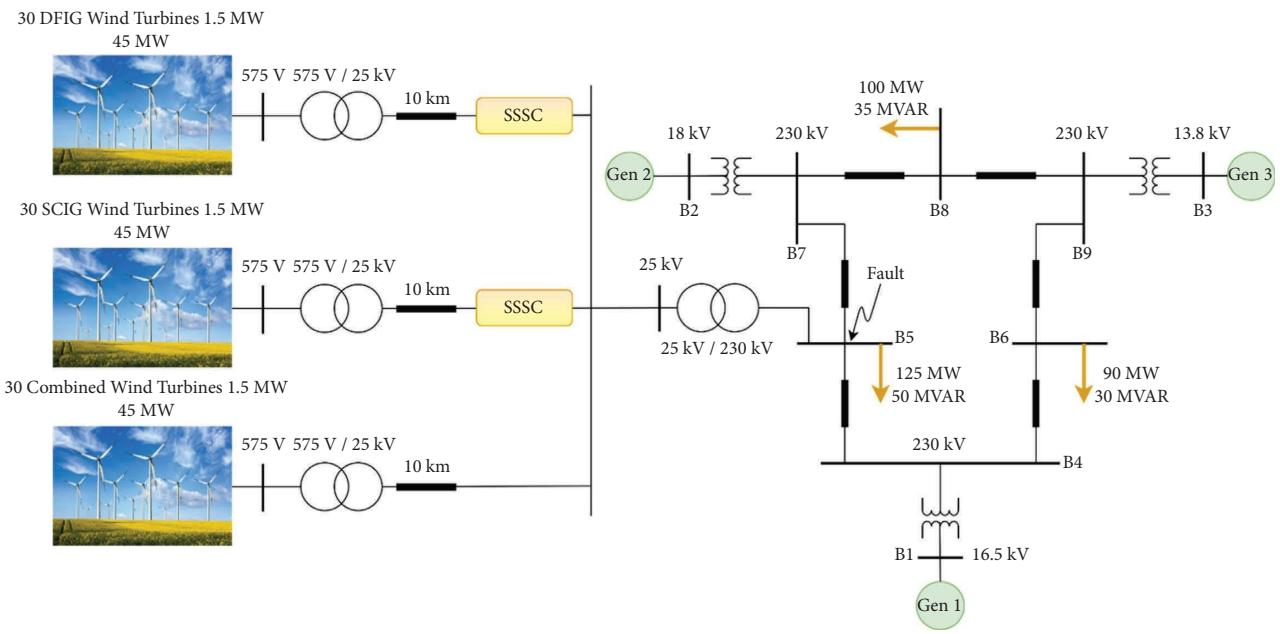

Figure 11: Schematic diagram of modified IEEE 9-bus test system integrated with a wind farm (System D).

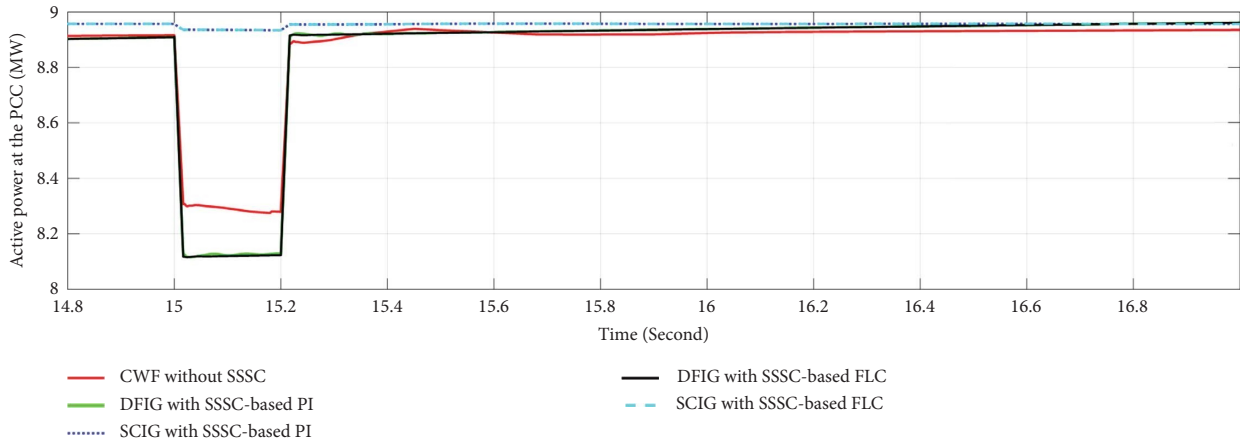

Figure 12: The effect of single-phase fault on the active power at the PCC.

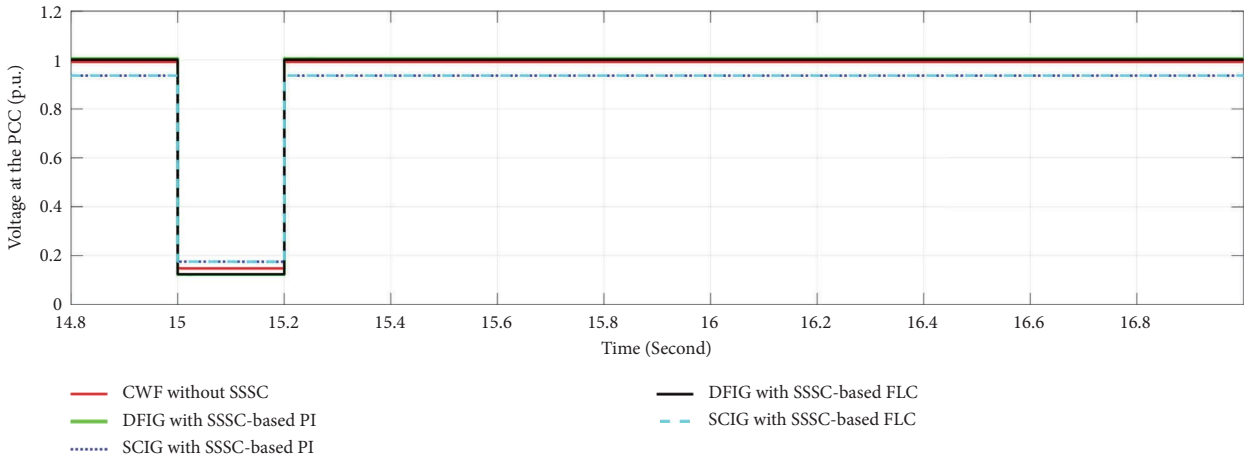

Figure 13: The effect of single-phase fault on voltage at the PCC.

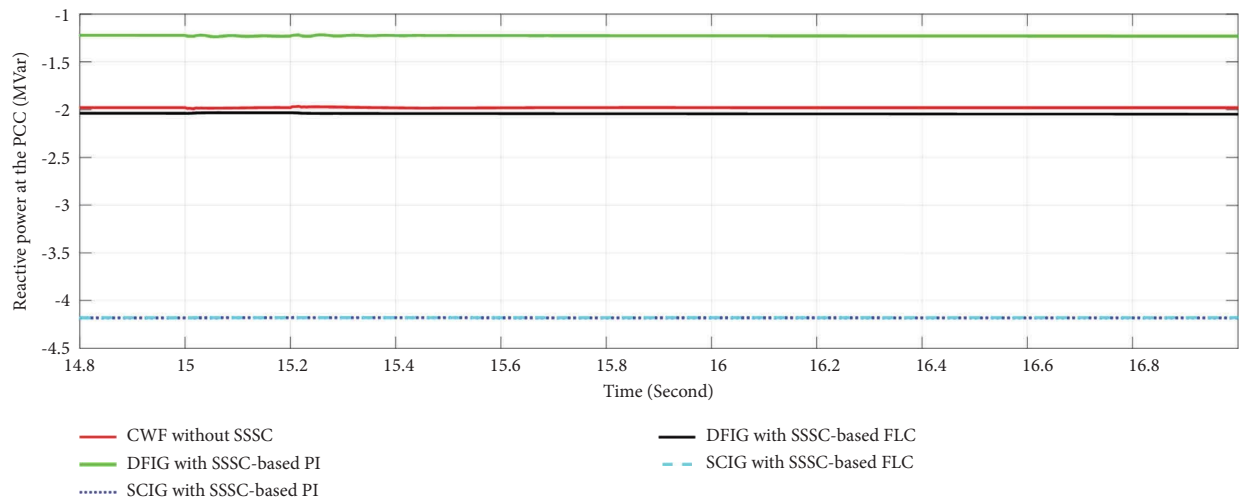

Figure 14: The effect of single-phase fault on the reactive power at the PCC.

least amount of reactive power from the grid. The CWF and DFIG wind farm with the SSSC-based FLC draw almost the same amount of reactive power. However, the SCIG wind farm draws the largest amount of reactive power. This is because in the case of DFIG-based wind farm, in addition to the SSSC, the converters used in the DFIGs also contribute to providing the required reactive power of wind turbines, whereas there is no converter in the SCIG-based wind farm.

6.2. Simulation Results for Three-Phase Fault on Systems A, B, and C

6.2.1. Active Power Variation. Figure 15 illustrates active power variation of the employed wind farms for a 0.2 seconds duration three-phase fault at bus B2, in Systems A, B, and C. Note that a three-phase fault is usually the most severe type of fault in power systems. As shown in Figure 15, active power of the SCIG wind farm falls to almost zero during the faulted period, and remains at this value until the end of simulation. As a result, the SCIG wind power plant is disconnected from the grid in the postfault state. It should be noted that basically an SCIG is not a robust generator, due to its constant speed characteristic and limited control over its output power. Thus, it may not be able to maintain its stability in the event of severe faults such as three-phase short circuit. For the SCIG-based wind farm, the SSSC was unable to improve the performance of wind turbine, either with the PI controller or with FLC.

On the other hand, active power of the DFIG wind turbine with the SSSC, whether equipped with a PI controller or with a FLC, quickly returns back to its prefault value (9 MW), in the postfault state. In fact, a DFIG is connected to the grid through a power electronic converter, and this makes it to be more flexible and controllable than an SCIG which is directly connected to the grid. However, the active power of the DFIG with SSSC-based FLC, experiences less oscillations in the postfault period compared to the DFIG with SSSC-based PI controller. As can be seen in Figure 15, for the DFIG wind farm with SSSC-based FLC, oscillations in the active power are damped out approximately 0.65 seconds faster than those of the DFIG wind farm with SSSC-based PI controller. It seems that the FLC improves the

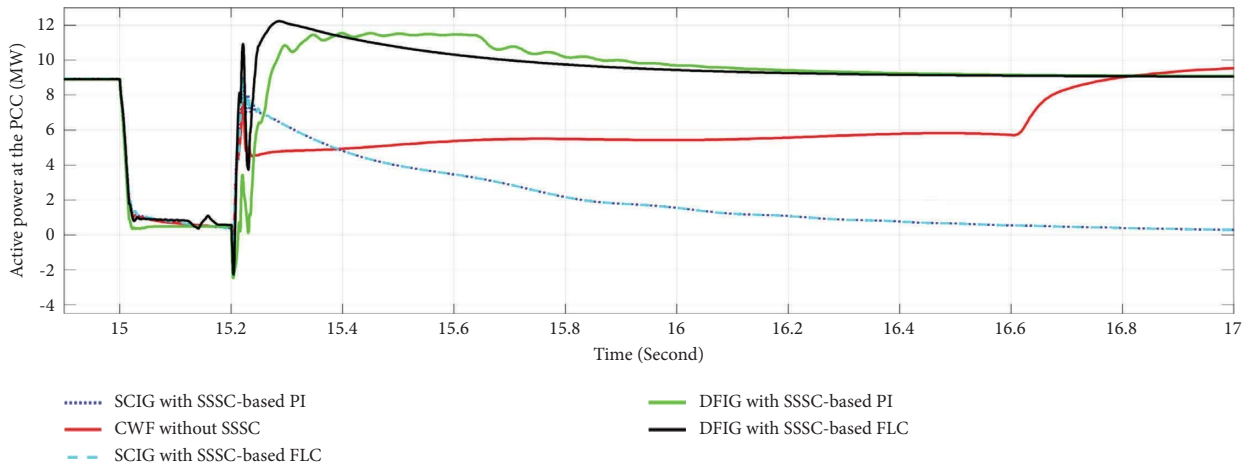

Figure 15: The effect of three-phase fault on the active power at the PCC.

SSSC performance, which in turn enhances the behavior of DFIG wind farm.

It can also be seen in Figure 15 that the CWF without SSSC is able to return back to its prefault steady-state condition in the postfault period. However, compared to the DFIG, it takes longer time for the CWF active power to reach its prefault value. The final conclusion is that, considering active power variation, the DFIG wind turbine with SSSC-based FLC, has the best performance under three-phase fault condition.

In Figure 16, active power variation of the DFIG and SCIG wind turbines in the CWF, for the assumed three-phase fault, are plotted separately. As seen in this figure, both DFIG and SCIG turbines can recover their active powers and stay connected to the grid, in the postfault period.

To further investigate the performance of SSSC-based FLC, we slightly changed the active power of the DFIG wind farm from its nominal value. Then, we re-simulated the behavior of the DFIG wind farm for the aforementioned three-phase fault. The obtained simulation results (not mentioned in this paper), showed that the DFIG wind farm with SSSC-based FLC can maintain its stability and remain connected to the grid in the postfault period. Therefore, it can be concluded that the SSSC-based FLC is able to maintain the stability of the wind farm even for those operating points that differ from the nominal operating conditions. In contrast, the DFIG wind farm with the SSSC-based PI controller failed to maintain its stability and disconnected from the grid.

Similarly, we investigated the performance of SSSC-based FLC in the SCIG wind farm, by changing the operating conditions of the SCIG. Again, the simulation results (not reported in this paper), showed that the SCIG wind farm with FLC-based SSSC can maintain its stability and stay connected to the grid in the postfault period. In contrast, the SCIG wind farm with the SSSC-based PI controller was unable to maintain its stability and was disconnected from the grid. Thus, we can conclude that the FLC is a robust controller against changes in the system operating conditions.

6.2.2. Terminal Voltage Variation. The terminal voltage variation at the PCC of wind farms for a three-phase fault of 0.2 seconds duration at bus B2 in Systems A, B, and C, is shown in Figure 17. As we can see in Figure 17, the terminal voltage in all the employed wind farms decreases drastically during the faulted period. However, all generators except the SCIG, recover their terminal voltages and reach stable states in the postfault period. After clearing the fault, the SCIG terminal voltage reaches 0.65 p.u., whereas it was 0.93 p.u. in the prefault system. Consequently, this generator cannot maintain its stability and is disconnected from the network.

The CWF can also recover its terminal voltage and its voltage quickly returns back to the prefault value of 1 p.u., in the postfault state. However, both the DFIG wind farm with SSSC-based FLC and the DFIG farm with SSSC-based PI controller can recover their terminal voltage much faster than other wind turbines. Furthermore, the DFIG with FLC has better performance than the DFIG with PI controller. In fact, the FLC causes the DFIG terminal voltage to experience less oscillations in the postfault period. Again, this confirms the superiority of the FLC over the PI controller. It can be seen in Figure 17 that for the DFIG wind farm, the FLC damps out the terminal voltage oscillations approximately 0.4 seconds faster than the PI controller.

Table 2 summarizes the results obtained in this subsection and in the previous subsection. In this table, the maximum overshoot in percent and settling time in seconds, for both active power and terminal voltage of all the studied wind farms, are given. As can be seen in Table 2, regarding both active power variation and terminal voltage variation, the DFIG wind farm with SSSC-based FLC, has the lowest settling time and can maintain its stability faster than other wind turbines in the postfault period.

6.2.3. Reactive Power Variation. The reactive power variation of the studied wind farms for a 0.2 seconds duration three-phase fault at bus B2 in Systems A, B, and C, is shown in Figure 18. It can be seen in Figure 18 that all wind turbines experience large variations in their reactive powers, during

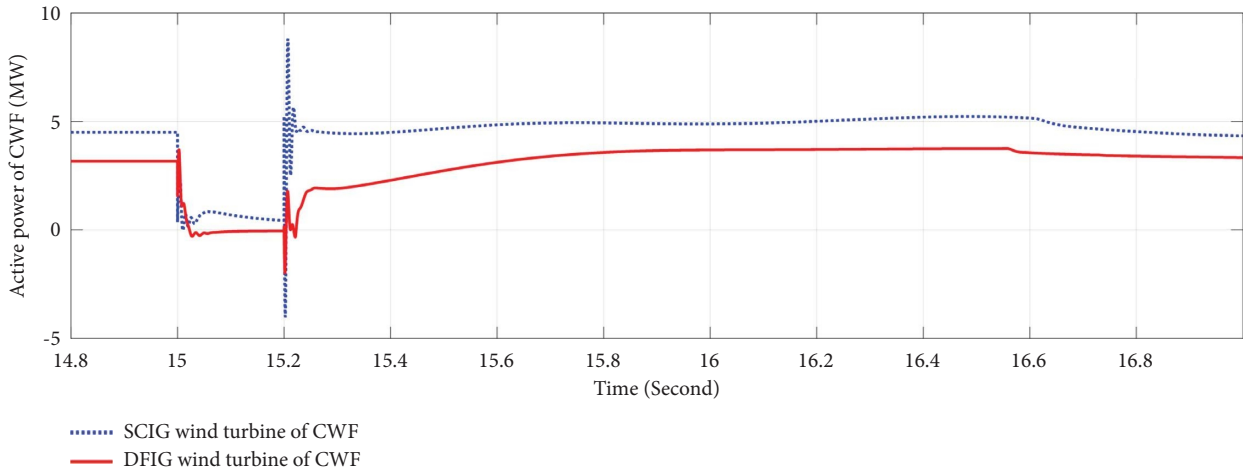

Figure 16: Active power of DFIG and SCIG wind turbines in CWF after three-phase fault.

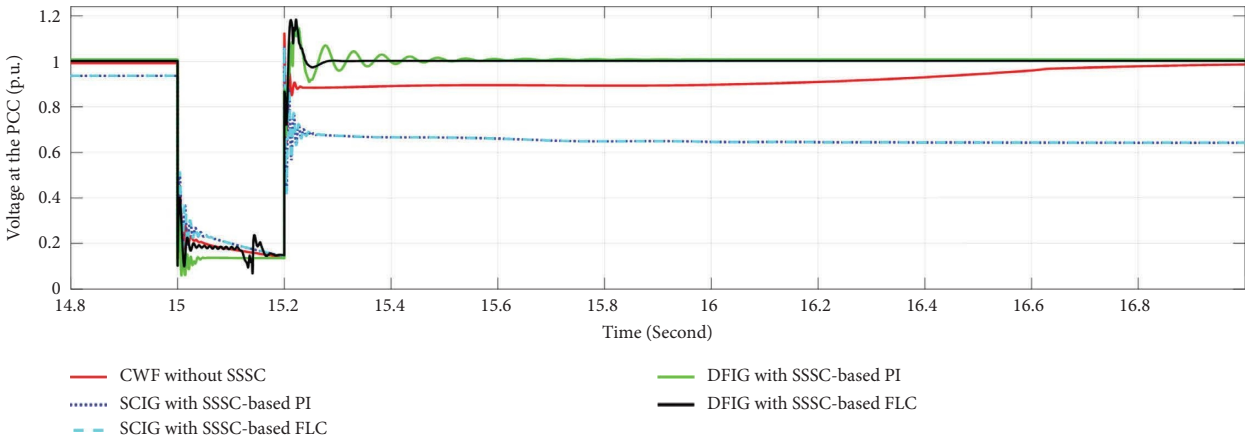

Figure 17: The effect of three-phase fault on voltage at the PCC.

Table 2: Maximum overshoot and settling time of active power and terminal voltage for three-phase fault.

Wind turbine/values	Active power		Terminal voltage	
	Maximum overshoot (%)/settling time (s)		Maximum overshoot (%)/settling time (s)	
DFIG with SSSC-FLC	35.07	16.22	18.49	15.26
DFIG with conventional SSSC	8.53	16.91	15.52	15.40
SCIG with SSSC-FLC	3.12	Disconnected	6.52	Unstable
SCIG with conventional SSSC	3.12	Disconnected	6.52	Unstable
CWF without SSSC	0	16.89	13.68	16.63

the faulted period. However, SCIG wind farms, both with SSSC-based FLC and SSSC-based PI controller, were unable to recover their reactive powers in the postfault state. As a matter of fact, due to high voltage drop in the system, the SCIG wind turbine needs to absorb a large amount of reactive power from the grid to recover in the postfault period. It seems that the network was unable to provide the reactive power required by the SCIG wind turbine, and as a result, it was disconnected from the grid.

The reactive powers of both the DFIG wind farm and the CWF reach their steady-state values in the postfault period. However, compared to the DFIG wind farm, the CWF needs a longer time to recover its reactive power. As shown in Figure 18, in the postfault state, the reactive power of the DFIG wind turbine with SSSC-based FLC recovers faster than other wind turbines. It can also be seen that compared to the DFIG with SSSC-based FLC, there are more oscillations in the reactive power of DFIG with SSSC-based PI controller. In other words, compared to the PI controller, the FLC has been able to improve the performance of SSSC more effectively. It can be seen in Figure 18 that for the DFIG wind farm, the FLC damps out reactive power oscillations approximately 0.6 seconds faster than the PI controller.

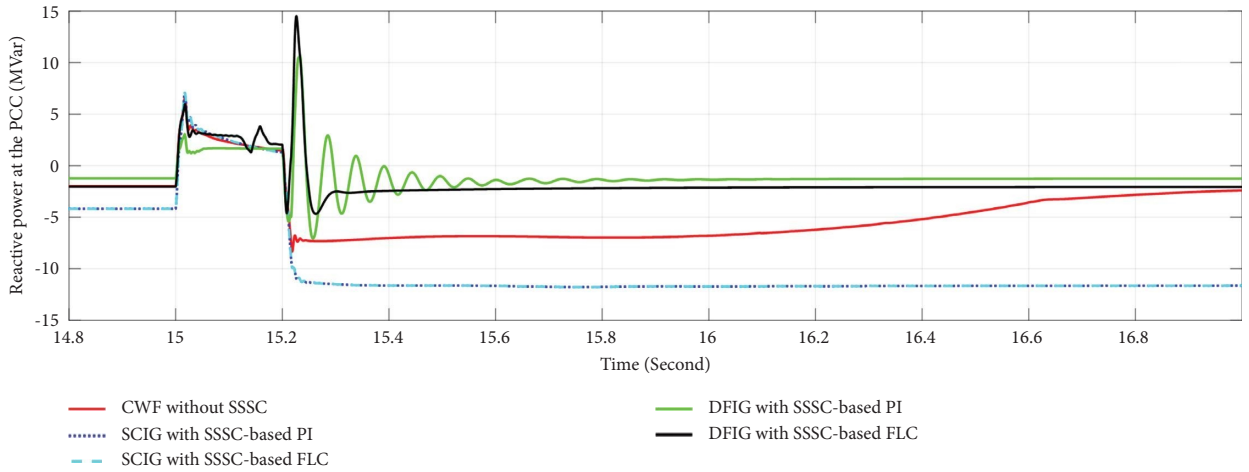

Figure 18: The effect of three-phase fault on the reactive power at the PCC.

In Figure 19, reactive power variation of the DFIG and SCIG wind turbines in the CWF, for the aforementioned three-phase fault, are plotted separately. It is seen in this figure that both the DFIG and SCIG turbines can recover their reactive powers and stay connected to the network, in the postfault state. As shown in Figure 19, the SCIG is drawing reactive power from the grid. In contrast, the DFIG is injecting reactive power to the grid. In fact, the AC/DC/AC converter is responsible for generating reactive power in the case of DFIG.

In Table 3, some values of the VSI for the DFIG-based wind farm, SCIG-based wind farm as well as CWF, are presented for the case of single-phase to ground fault. For the DFIG wind farm, the VSI is less than 1 from the initiation of fault (i.e., $t = 15$ seconds) to $t = 15.05$ seconds, which means the voltage is unstable during this time duration. However, the VSI is greater than 1 after $t = 15.15$ seconds and remains greater than 1 until the end of simulation. This verifies that the transmission line is being used within its permissible power range in the postfault state. For both the SCIG wind farm and CWF, similar results were obtained for the VSI. Therefore, regarding voltage stability and considering single-phase fault, all the employed wind farms had almost the same behavior.

Some values of the VSI for the three-phase fault are also given in Table 3. As can be seen in Table 3, the VSI for the DFIG wind farm is less than 1 from the initiation of fault (i.e., $t = 15$ seconds) to $t = 15.15$ seconds, meaning that the voltage is unstable during this time duration. The VSI is greater than 1 from $t = 15.25$ seconds until the end of simulation, indicating that in the postfault state, the transmission line is being used within its permissible power range. The VSI for the SCIG wind farm is less than 1 until $t = 15.25$ seconds. From $t = 15.35$ seconds until the end of simulation time, the VSI is greater than 1, which indicates the transmission line is being used within its permissible power range. The VSI for the CWF is also greater than 1 from $t = 15.35$ seconds until the end of simulation, which again means the transmission line is being operated within its permissible power range. These results show that the DFIG wind farm is able to regain its voltage stability faster than both the SCIG wind farm and CWF. In fact, the simulation results show that in comparison with the DFIG, it takes approximately 0.30 seconds longer for the SCIG wind farm and CWF to recover in the postfault period. In other words, the performance of the DFIG wind farm equipped with either SSSC-based FLC or SSSC-based PI controller was better than other wind farms, for three-phase fault condition.

6.3. Simulation Results for Three-Phase Fault on System D (IEEE 9-Bus)

6.3.1. Active Power Variation. In this section, it is assumed that a three-phase fault of 0.2 seconds duration occurs at the PCC (i.e., bus B5) in System D (IEEE 9-bus system). As shown in Figure 20, active power of the SCIG wind farm falls to zero during the faulted period, and remains at this value until the end of simulation. Consequently, the SCIG wind power plant is disconnected from the grid in the postfault state. For the SCIG wind turbine, the SSSC was unable to improve the performance of SCIG, either with the PI controller or with the fuzzy logic controller.

On the other hand, oscillation in the active power of DFIG wind turbine with an SSSC, whether equipped with a PI controller or with a fuzzy logic controller, quickly decays after clearing the fault. As mentioned before, a DFIG is connected to the grid through a power electronic converter, which makes it to be more flexible and controllable than an SCIG that is connected to the grid directly. However, compared to the DFIG with SSSC-based PI controller, the active power of the DFIG with SSSC-based FLC experiences less oscillations in the postfault period. As can be seen in Figure 20, for the DFIG wind farm, the FLC damps out active power oscillations approximately 0.9 seconds faster than the PI controller. It can be concluded that the FLC improves the SSSC performance, which in turn enhances the behavior of the DFIG wind farm.

It can also be seen in Figure 20 that the CWF without SSSC stay connected to the grid, in the postfault period. However, compared to the DFIG wind farm, the CWF needs

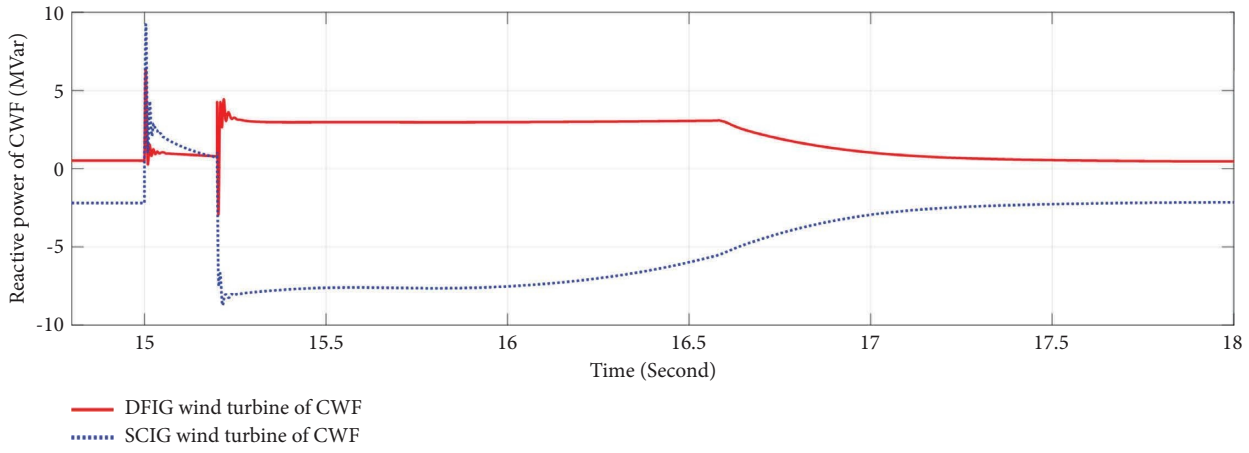

Figure 19: Reactive power of DFIG and SCIG wind turbine in CWF after three-phase fault.

Table 3: Some values for VSI in the employed wind farms after both single-phase fault and three-phase fault.

Wind turbine/time (sec.)	15.03	15.05	15.15	15.25	15.35	15.45	15.55	16.00
Single-phase fault								
DFIG with SSSC-FLC	VSI < 1	VSI < 1	VSI > 1	VSI > 1	VSI > 1	VSI > 1	VSI > 1	VSI > 1
DFIG with conventional SSSC	VSI < 1	VSI < 1	VSI > 1	VSI > 1	VSI > 1	VSI > 1	VSI > 1	VSI > 1
SCIG with SSSC-FLC	VSI < 1	VSI < 1	VSI > 1	VSI > 1	VSI > 1	VSI > 1	VSI > 1	VSI > 1
SCIG with conventional SSSC	VSI < 1	VSI < 1	VSI > 1	VSI > 1	VSI > 1	VSI > 1	VSI > 1	VSI > 1
CWF without SSSC	VSI < 1	VSI < 1	VSI > 1	VSI > 1	VSI > 1	VSI > 1	VSI > 1	VSI > 1
Three-phase fault								
DFIG with SSSC-FLC	VSI < 1	VSI < 1	VSI < 1	VSI > 1	VSI > 1	VSI > 1	VSI > 1	VSI > 1
DFIG with conventional SSSC	VSI < 1	VSI < 1	VSI < 1	VSI > 1	VSI > 1	VSI > 1	VSI > 1	VSI > 1
SCIG with SSSC-FLC	VSI < 1	VSI < 1	VSI < 1	VSI < 1	VSI > 1	VSI > 1	VSI > 1	VSI > 1
SCIG with conventional SSSC	VSI < 1	VSI < 1	VSI < 1	VSI < 1	VSI > 1	VSI > 1	VSI > 1	VSI > 1
CWF without SSSC	VSI < 1	VSI < 1	VSI < 1	VSI < 1	VSI > 1	VSI > 1	VSI > 1	VSI > 1

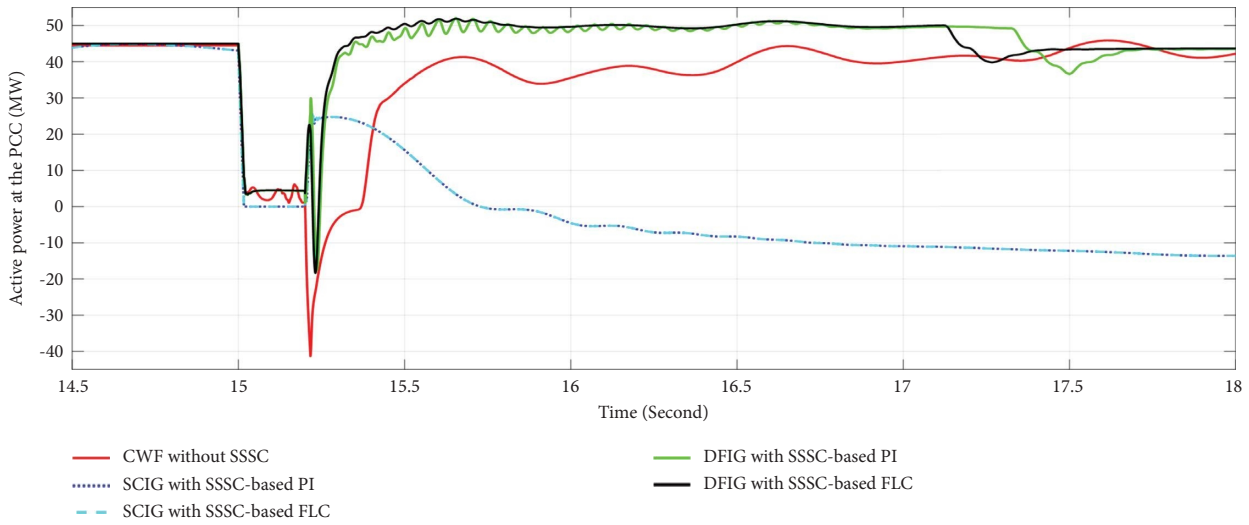

Figure 20: The effect of three-phase fault on the active power at PCC of IEEE 9-bus system.

a longer time to recover its active power. Therefore, it can be concluded that regarding active power variation and for the three-phase fault conditions, the DFIG wind farm with SSSC-based FLC, had the best performance among other wind farms.

6.3.2. Terminal Voltage Variation. The terminal voltage variation of the wind farms for a three-phase fault of 0.2 seconds duration at bus B5 in the IEEE-9 bus system (System D) is shown in Figure 21. As we can see in Figure 21, the terminal voltage in all the employed wind farms decreases drastically during the faulted period. However, all generators except the SCIG, recover their terminal voltages and reach stable states in the postfault period. After clearing the fault, the terminal voltage of SCIG reaches 0.77 p.u., whereas it was 0.95 p.u. in the prefault system. As a result, this generator cannot maintain its stability and is disconnected from the grid.

The CWF is also able to recover its terminal voltage and its voltage quickly returns back to the prefault value of 1 p.u., in the postfault period. However, both the DFIG wind farm with SSSC-based FLC and the DFIG farm with SSSC-based PI controller can recover their terminal voltage much faster than other wind turbines. Moreover, the DFIG with FLC has better performance than the DFIG with PI controller. As a matter of fact, the FLC causes the DFIG terminal voltage to experience less oscillations in the postfault period. This again confirms the superiority of the FLC over the PI controller. It is seen in Figure 21 that for the DFIG wind farm, the FLC damps out terminal voltage oscillations approximately 0.8 seconds faster than the PI controller.

Table 4 summarizes the results obtained in this subsection and in the previous subsection. In this table, the maximum overshoot in percent, and settling time in seconds, for both active power and terminal voltages of all the studied wind farms in the IEEE 9-bus system, are given. As can be seen in Table 4, regarding active power variation and terminal voltage variation, the CWF without SSSC has the lowest outshoot. In addition, regarding terminal voltage variation, the CWF has the lowest settling time and can maintain its stability faster than other wind turbines in the postfault state. It can also be seen that considering active power variation and terminal voltage variation, the DFIG wind farm with SSSC-based FLC has better performance than the DFIG wind farm with SSSC-based PI controller.

6.3.3. Reactive Power Variation. The reactive power variation of the studied wind farms for a three-phase fault of 0.2 seconds duration at bus B5 in System D (IEEE 9-bus system), is shown in Figure 22. It can be seen in Figure 22 that all the wind turbines experience large variations in their reactive powers, in the faulted period. However, the SCIG wind farms, both with SSSC-based FLC and with SSSC-based PI controller, are unable to recover their reactive powers in the postfault state. As previously explained, due to high voltage drop in the postfault system, the SCIG wind turbine needs to draw a large amount of reactive power from the grid to recover. The network was unable to provide the required reactive power of the SCIG wind turbine; thus, it was disconnected from the grid.

The reactive powers of both the DFIG wind farm and the CWF reach their steady-state values in the postfault period. However, the reactive power of the CWF recovers faster than other wind turbines in the postfault state. It can also be seen that compared to the DFIG with SSSC-based FLC there are more oscillations in the reactive power of DFIG with SSSC-based PI controller. This confirms that in comparison with the PI controller, the FLC has been able to improve the performance of SSSC more effectively. It is seen in Figure 22 that for the DFIG wind farm, the FLC damps out reactive power oscillations approximately 1.1 seconds faster than the PI controller.

6.4. Simulation Results for Line-to-Line Fault on System D (IEEE 9-Bus)

6.4.1. Active Power Variation. In this section, we assume that a line-to-line fault of 0.2 seconds duration occurs at the PCC (i.e., bus B5) in System D (IEEE 9-bus system). As shown Figure 23, all the wind turbines experience large variations in their active powers in the faulted period. It is seen in Figure 23 that active power of the SCIG wind farm with SSSC-based PI controller cannot be recovered; therefore, this wind farm is disconnected from the grid in the postfault state. In contrast, the SCIG wind farm with SSSC-based FLC recovered its active power and stayed connected to the grid. In addition, oscillation in the active power of DFIG wind turbine with the SSSC, whether equipped with a PI controller or with a FLC, quickly decays after clearing the fault. However, the active power of the CWF recovered faster than other wind turbines. Therefore, it can be concluded that regarding active power variation and in the event of line-to-line fault, the CWF has the best performance among other wind farms.

6.4.2. Terminal Voltage Variation. The terminal voltage variation of the wind farms for a line-to-line fault of 0.2 seconds duration at bus B5 in the IEEE-9 bus system (System D) is shown in Figure 24. We can see in Figure 24 that terminal voltage in all the employed wind farms is greatly reduced during the faulted period. However, all the wind generators except the SCIG with SSSC-based PI controller recovered their terminal voltage and reached stable states in the postfault period. Furthermore, oscillation in the terminal voltage of DFIG wind turbine with SSSC, whether equipped with a PI controller or with a FLC, quickly decays in the postfault state. Nevertheless, the CWF terminal voltage recovered faster than other wind turbines. Consequently, we can conclude that regarding terminal voltage variation and for the case of line-to-line fault, the CWF has the best performance among other wind farms.

6.4.3. Reactive Power Variation. The reactive power variation of the wind farms for a line-to-line fault of 0.2 seconds duration at bus B5 in System D (IEEE 9-bus system), is

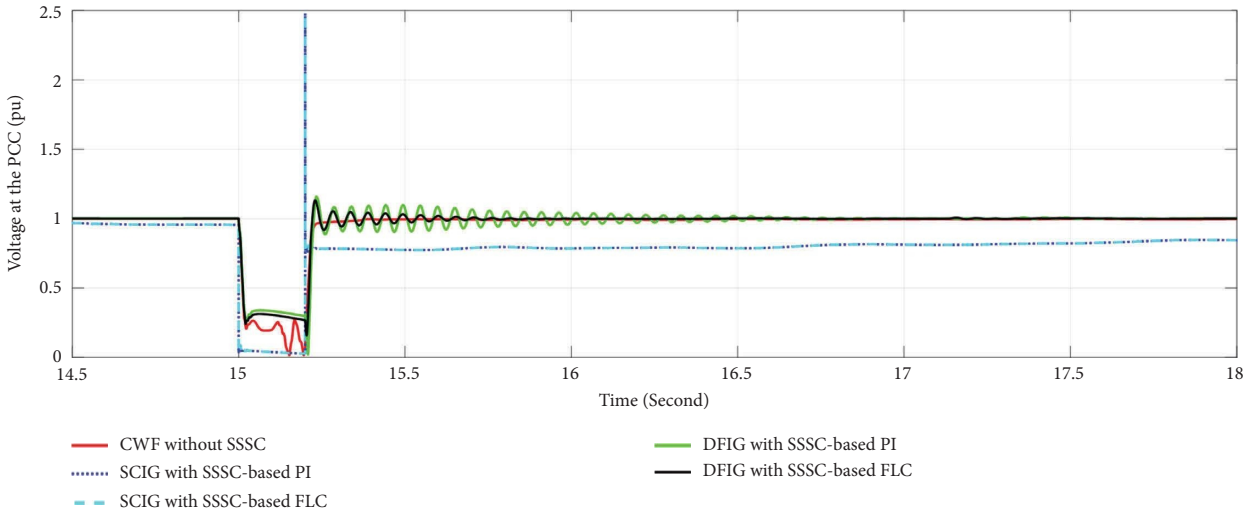

Figure 21: The effect of three-phase fault on the voltage at PCC of IEEE 9-bus system.

Table 4: Maximum overshoot and settling time of active power and terminal voltage in IEEE 9-bus system.

Wind turbine/values	Active power		Terminal voltage	
	Maximum overshoot (%)/settling time (s)		Maximum overshoot (%)/settling time (s)	
DFIG with SSSC-FLC	18.84	17.38	13.42	15.57
DFIG with conventional SSSC	18.98	17.73	13.44	15.60
SCIG with SSSC-FLC	9.48	Disconnected	1.52	Unstable
SCIG with conventional SSSC	9.48	Disconnected	1.52	Unstable
CWF without SSSC	8.60	17.94	1.48	15.28

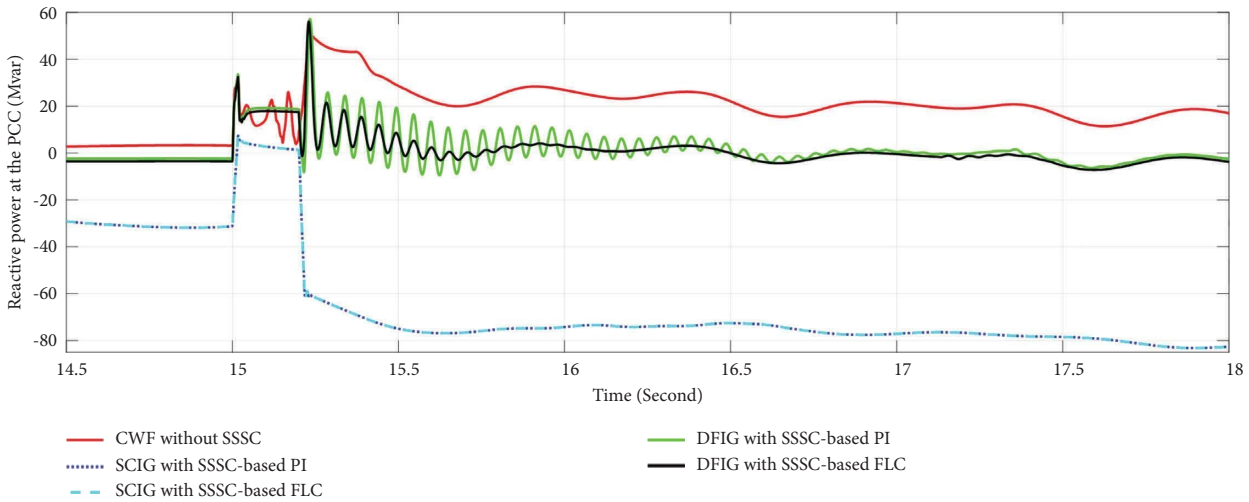

Figure 22: The effect of three-phase fault on the reactive power at PCC of IEEE 9-bus system.

shown in Figure 25. It can be seen in Figure 25 that all the wind turbines experience large variations in their reactive powers, in the faulted period. However, the SCIG wind farm with SSSC-based PI controller was unable to recover its reactive power and was disconnected from the grid in the postfault system. It can also be seen in Figure 25 that the FLC employed for the SSSC in SCIG wind turbine, improved the behavior of this wind turbine; therefore, the SCIG wind farm with SSSC-based FLC was able to recover its reactive power in the postfault state.

The reactive powers of both the DFIG wind farm and the CWF reach their steady-state values in the postfault period. However, the reactive power of the CWF recovered faster than other wind turbines. In addition, it is seen in Figure 25

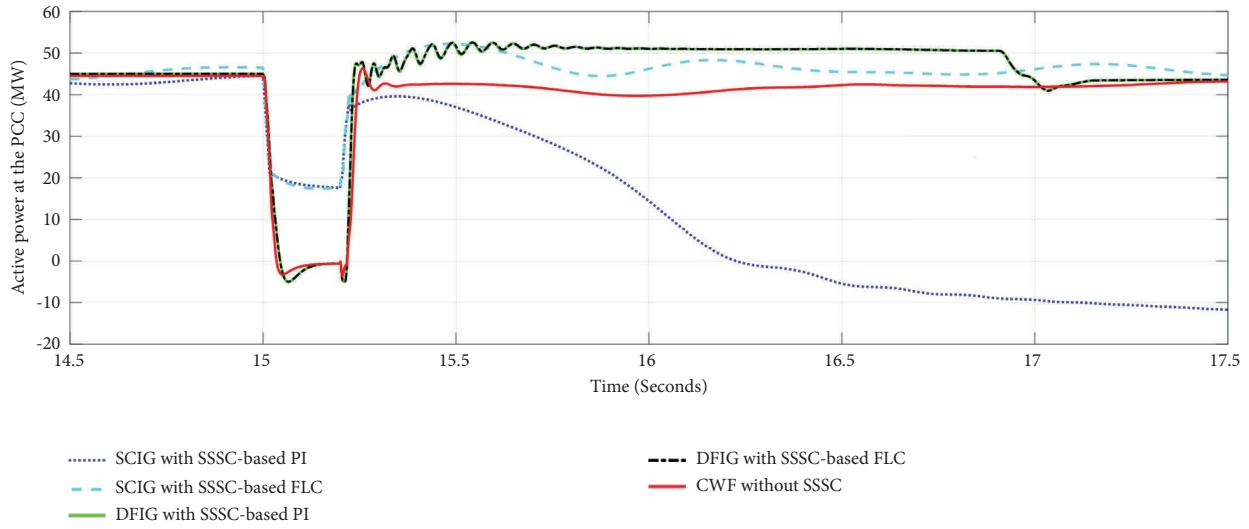

Figure 23: The effect of line-to-line fault on the active power at PCC of IEEE 9-bus system.

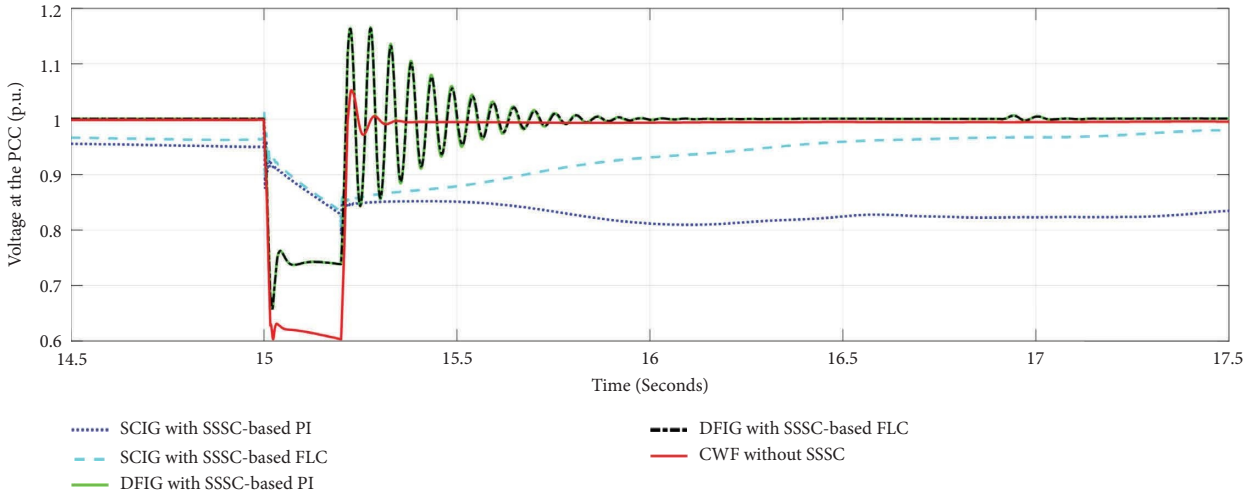

Figure 24: The effect of line-to-line fault on the voltage at PCC of IEEE 9-bus system.

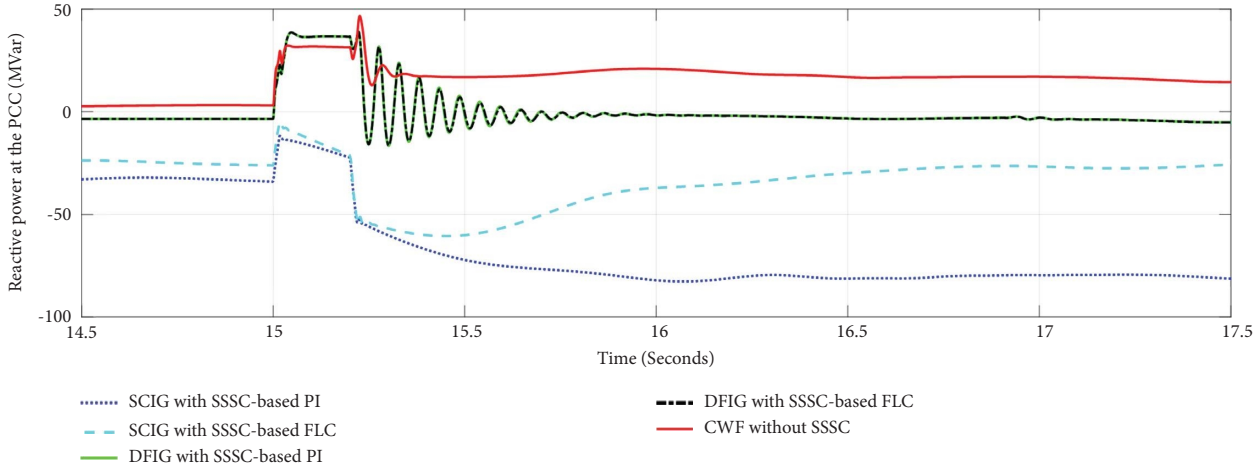

Figure 25: The effect of line-to-line fault on the reactive power at PCC of IEEE 9-bus system.

Table 5: The SCIG, DFIG, and SSSC parameters in the studied systems.

SSSC	Value	SCIG	Value	DFIG	Value
Rating	100×10^6 VA	Maximum power at nominal wind speed	1.5 MW	Maximum power at nominal wind speed	1.5 MW
Nominal line voltage	25 kV	Nominal voltage	575 V	Nominal voltage	575 V
Nominal frequency	60 Hz	Nominal frequency	60 Hz	Nominal frequency	60 Hz
DC link normal voltage	1200 V	Stator resistance	0.004843 p.u.	Stator resistance	0.00706 p.u.
DC link total equivalent capacitance	100×10^{-6} F	Rotor resistance	0.004377 p.u.	Rotor resistance	0.005 p.u.
Series converter resistance	0.0053 p.u.	Stator leakage inductance	0.1248 p.u.	Stator leakage inductance	0.171 p.u.
Series converter inductance	0.16 p.u.				

that in comparison to the DFIG with SSSC-based FLC, there exist more oscillations in the reactive power of DFIG with SSSC-based PI controller. Therefore, compared to the PI controller, the FLC has been able to improve the performance of SSSC more effectively in the DFIG wind farm.

7. Discussion

The method proposed in this paper was implemented on two test power systems; however, it can be applied to any other power system in a similar way. It should be noted that in both test systems, the wind farms were assumed to be connected to a transmission system through a short transmission line (or a radial distribution feeder). In the first test system, the wind farms are connected through a 25 km distribution feeder to a grid that actually represents an infinite bus. In the second test system, the wind farms are connected to a load bus in the IEEE 9-bus system through a 10 km feeder. However, wind farms can also be utilized in large distribution systems such as the IEEE 123-bus test power distribution system [52]. Furthermore, wind farms in a large distribution system can be connected to a transmission system through a distribution feeder [53]. In such cases, the wind farms are indeed connected to a hybrid transmission-distribution power system. In a hybrid system, a compensator such as the SSSC can also be used in distribution feeders connecting the wind farms to the transmission system to enhance the dynamic performance of the system. In addition, to improve the efficacy of the SSSC, it can be equipped with a fuzzy logic controller. It should be noted that the design and parameters setting of the fuzzy logic controller in such a hybrid system could be a difficult task. In this paper, the faults were assumed to occur at only one location in the test systems. However, we can make a better assessment for the performance of the proposed SSSC by considering different fault locations in the studied systems. It can be assumed that in addition to the distribution level, faults also occur at the transmission level in the hybrid system, so that the behavior of both the wind farms and the synchronous generators could be investigated. It is also suggested to evaluate the performance of SSSC and its fuzzy logic controller by changing both the wind energy penetration level in the distribution system and the output powers of synchronous generators in the transmission system. Investigating all these issues could be considered as future research works.

8. Conclusion

Nowadays, wind energy plays an important and growing role in the electric power systems and its penetration level is increasing. However, the integration of wind energy into the power systems may affect the dynamic performance of power systems. To improve the performance of power systems integrated with wind farms, some compensators are usually employed. In this article, the behavior of power systems connected to squirrel cage induction generator-(SCIG-) based wind farm, doubly-fed induction generator-(DFIG-) based wind farm, and combined wind farm (CWF), was examined under short-circuit faults conditions. A CWF consists of an equal number of both generators, i.e., SCIG and SCIG. For the wind farms based on the SCIG and DFIG, a static synchronous series compensator (SSSC) was also utilized. Furthermore, a fuzzy logic controller (FLC) as well as a conventional (PI) controller was used for the SSSC in the studied systems. The method proposed in this paper was implemented on two test power systems. The first system is a simple system that includes a 9 MW wind farm connected to the grid, and the second system is the IEEE 9-bus test system which is integrated with a 45 MW wind farm. To evaluate the effectiveness of the proposed approach, the time variation of wind farms terminal voltage, active power, and reactive power, along with a voltage stability index (VSI), were monitored in the event of faults in the studied systems. All simulations were carried out in MATLAB/Simulink software. The obtained simulation results are summarized as follows:

(i) Single-phase to ground fault

In both systems, the performance of the SCIG wind farm, either with SSSC-based FLC or with SSSC-based PI controller, was better than the CWF and DFIG wind farm. Compared with the CWF and DFIG wind farm, the SCIG wind farm took less time to recover in the postfault period. Nevertheless, the SCIG wind farm absorbed more reactive power from the network to maintain its stability. In addition, both the CWF and DFIG wind farm were also able to stay connected to the grid.

(ii) Three-phase fault

The SCIG wind farm was disconnected from the grid in both systems. For the SCIG wind farm, the SSSC was unable to improve the performance of wind turbine, either with the PI controller or with the FLC. Both the CWF and the DFIG wind turbine were able to stay connected to the grid in the postfault period. However, the DFIG wind turbine with SSSC-based FLC had the best performance in both systems. The results obtained also indicated that in the IEEE 9-bus system, the FLC was able to damp out wind farms terminal voltage oscillations, active power oscillations and reactive power oscillations by 0.8, 0.9, and 1.1 seconds, respectively, faster than the PI controller.

(iii) Line-to-Line fault

The line-to-line fault was considered only in the IEEE 9-bus system. The SCIG wind farm with SSSC-based PI controller was unable to stay connected to grid; however, the SCIG wind farm with SSSC-based FLC was able to maintain its stability. Both the CWF and the DFIG wind turbine stay connected to the grid in the postfault state. Nevertheless, the CWF had the best performance among other wind farms.

The obtained results showed that although an SSSC together with a PI controller or a FLC can improve the performance of the SCIG- and DFIG-based wind farms, the

CWF wind farm also has proper and acceptable dynamic performance. Therefore, a power system could be integrated with a CWF without any additional costs and/or using any compensators. In this article, all noises and measurement errors have been ignored. Future research can be focused on considering these errors in the proposed method.

Appendix

This section presents Table 5, which gives the parameters of SCIG, DFIG, and SSSC in the studied systems.

Data Availability

The data used to support the findings of this study are included within the article.

Conflicts of Interest

The authors declare that they have no conflicts of interest.

Authors' Contributions

Ahmadreza Abdollahi Chirani performed investigation, proposed the methodology, provided software, wrote the original draft, reviewed and edited the article, visualized the study, contributed to validation, and performed formal analysis. A. Karami performed investigation, performed supervision, reviewed and edited the article, and provided project administration.

References

[1] R. Hemmati, H. Faraji, and N. Y. Beigvand, "Multi objective control scheme on DFIG wind turbine integrated with energy storage system and FACTS devices: steady-state and transient operation improvement," *International Journal of Electrical Power & Energy Systems*, vol. 135, Article ID 107519, 2022.

[2] A. Chakraborty and T. Maity, "A novel application of adaptive filtering algorithm for LVRT capability enhancement of grid-connected DFIG-based wind energy conversion systems (WECS)," *Electric Power Systems Research*, vol. 217, Article ID 109179, 2023.

[3] R. K. Samal and M. Tripathy, "A novel distance metric for evaluating impact of wind integration on power systems," *Renewable Energy*, vol. 140, pp. 722–736, 2019.

[4] P. He, M. Zheng, H. Jin, Z. Gong, and J. Dong, "Introducing MRAC-PSS-VI to increase small-signal stability of the power system after wind power integration," *International Transactions on Electrical Energy Systems*, vol. 2022, pp. 1–20, Article ID 3525601, 2022.

[5] J. Bhukya and V. Mahajan, "Parameter tuning of PSS and STATCOM controllers using genetic algorithm for improvement of small-signal and transient stability of power systems with wind power," *International Transactions on Electrical Energy Systems*, vol. 31, no. 7, Article ID e12912, 2021.

[6] H. Benbouhenni, N. Bizon, M. I. Mosaad, I. Colak, A. B. Djilali, and H. Gasmi, "Enhancement of the power quality of DFIG-based dual-rotor wind turbine systems using fractional order fuzzy controller," *Expert Systems with Applications*, vol. 238, Article ID 121695, 2024.

[7] Z. H. Liu, C. T. Wang, H. L. Wei, B. Zeng, M. Li, and X. P. Song, "A wavelet-LSTM model for short-term wind power forecasting using wind farm SCADA data," *Expert Systems with Applications*, vol. 247, Article ID 123237, 2024.

[8] C. Li, Y. Cao, B. Li, S. Wang, and P. Chen, "A novel power control scheme for distributed DFIG based on cooperation of hybrid energy storage system and grid-side converter," *International Journal of Electrical Power & Energy Systems*, vol. 157, Article ID 109801, 2024.

[9] M. Ahmadi Kamarposhti, H. Shokouhandeh, Y. Gholami Omali, I. Colak, P. Thounthong, and W. Holderbaum, "Optimal coordination of TCSC and PSS2B controllers in electric power systems using MOPSO multiobjective algorithm," *International Transactions on Electrical Energy Systems*, vol. 2022, Article ID 5233620, 18 pages, 2022.

[10] M. G. Jolfaei, A. M. Sharaf, S. M. Shariatmadar, and M. B. Poudeh, "A hybrid PSS–SSSC GA-stabilization scheme for damping power system small signal oscillations," *International Journal of Electrical Power & Energy Systems*, vol. 75, pp. 337–344, 2016.

[11] J. Qi, W. Zhao, and X. Bian, "Comparative study of SVC and STATCOM reactive power compensation for prosumer microgrids with DFIG-based wind farm integration," *IEEE Access*, vol. 8, pp. 209878–209885, 2020.

[12] H. Kuang, L. Zheng, S. Li, and X. Ding, "Voltage stability improvement of wind power grid-connected system using TCSC-STATCOM control," *IET Renewable Power Generation*, vol. 13, no. 2, pp. 215–219, 2019.

[13] N. A. Lahaçani, D. Aouzellag, and B. Mendil, "Contribution to the improvement of voltage profile in electrical network with wind generator using SVC device," *Renewable Energy*, vol. 35, no. 1, pp. 243–248, 2010.

[14] V. Kumar, A. S. Pandey, and S. K. Sinha, "Stability improvement of DFIG-based wind farm integrated power system using ANFIS controlled STATCOM," *Energies*, vol. 13, no. 18, p. 4707, 2020.

[15] T. R. Ayodele, "Comparative assessment of SVC and TCSC controllers on the small signal stability margin of a power system incorporating intermittent wind power generation," *Journal of Wind Energy*, vol. 2014, Article ID 570234, 12 pages, 2014.

[16] M. Abdelsattar, W. Arafa Hafez, A. A Elbaset et al., "Voltage stability improvement of an Egyptian power grid-based wind energy system using STATCOM," *Wind Energy*, vol. 25, no. 6, pp. 1077–1120, 2022.

[17] J. Bhukya and V. Mahajan, "Optimization of damping controller for PSS and SSSC to improve stability of interconnected system with DFIG based wind farm," *International Journal of Electrical Power & Energy Systems*, vol. 108, pp. 314–335, 2019.

[18] D. N. Truong and V. T. Ngo, "Designed damping controller for SSSC to improve stability of a hybrid offshore wind farms considering time delay," *International Journal of Electrical Power & Energy Systems*, vol. 65, pp. 425–431, 2015.

[19] S. R. Khuntia and S. Panda, "ANFIS approach for SSSC controller design for the improvement of transient stability performance," *Mathematical and Computer Modelling*, vol. 57, no. 1-2, pp. 289–300, 2013.

[20] P. Y. Grachev, A. S. Tabachinskiy, and P. Kanagavel, "New stator construction and simulation of high-efficiency wind turbine generators," *IEEE Transactions on Industry Applications*, vol. 56, no. 2, pp. 1389–1396, 2020.

[21] Y. Kailasa Gounder, D. Nanjundappan, and V. Boominathan, "Enhancement of transient stability of distribution system with SCIG and DFIG based wind farms using STATCOM," *IET Renewable Power Generation*, vol. 10, no. 8, pp. 1171–1180, 2016.

[22] M. J. Hossain, H. R. Pota, and R. A. Ramos, "Robust STATCOM control for the stabilisation of fixed-speed wind turbines during low voltages," *Renewable Energy*, vol. 36, no. 11, pp. 2897–2905, 2011.

[23] Y. Nie, J. Zhang, T. Liu, J. Cui, and L. Zhang, "Low-voltage ride-through handling in wind farm with doubly fed induction generators based on variable-step model predictive control," *IET Renewable Power Generation*, vol. 17, no. 8, pp. 2101–2112, 2023.

[24] M. Firouzi, G. B. Gharehpetian, and Y. Salami, "Active and reactive power control of wind farm for enhancement transient stability of multi-machine power system using UIPC," *IET Renewable Power Generation*, vol. 11, no. 8, pp. 1246–1252, 2017.

[25] A. El-Sattar, N. Saad, and M. S. El-Dein, "Dynamic response of doubly fed induction generator variable speed wind turbine under fault," *Electric Power Systems Research*, vol. 78, no. 7, pp. 1240–1246, 2008.

[26] N. N. Shah and S. R. Joshi, "Modal analysis for selection of DFIG-based wind farms for damping and reduction of the risk of SSR," *IET Energy Systems Integration*, vol. 1, no. 4, pp. 252–268, 2019.

[27] N. Senthil Kumar and J. Gokulakrishnan, "Impact of FACTS controllers on the stability of power systems connected with doubly fed induction generators," *International Journal of Electrical Power & Energy Systems*, vol. 33, no. 5, pp. 1172–1184, 2011.

[28] O. Noureldeen, M. Rihan, and B. Hasanin, "Stability improvement of fixed speed induction generator wind farm using STATCOM during different fault locations and durations," *Ain Shams Engineering Journal*, vol. 2, no. 1, pp. 1–10, 2011.

[29] A. Rashad, S. Kamel, and F. Jurado, "Stability improvement of power systems connected with developed wind farms using SSSC controller," *Ain Shams Engineering Journal*, vol. 9, no. 4, pp. 2767–2779, 2018.

[30] O. Noureldeen and A. Rashad, "Modeling and investigation of Gulf El-Zayt wind farm for stability studying during extreme gust wind occurrence," *Ain Shams Engineering Journal*, vol. 5, no. 1, pp. 137–148, 2014.

[31] M. Kayikçi and J. Milanovic, "Assessing transient response of DFIG-based wind plants—the influence of model simplifications and parameters," *IEEE Transactions on Power Systems*, vol. 23, no. 2, pp. 545–554, 2008.

[32] J. Justo, F. Mwasilu, and J. Jung, "Effective protection for doubly fed induction generator-based wind turbines under three-phase fault conditions," *Electrical Engineering*, vol. 100, no. 2, pp. 543–556, 2018.

[33] O. E. M. Youssef, M. G. Hussien, and A. E. W. Hassan, "An advanced control performance of a sophisticated stand-alone wind-driven DFIG system," *International Transactions on Electrical Energy Systems*, vol. 2023, Article ID 5541932, 11 pages, 2023.

[34] A. Mohammad Nezhad, B. Tousi, and F. Sabahi, "Power control of a grid-connected doubly fed induction generator using H∞ control and Kalman filter," *International Transactions on Electrical Energy Systems*, vol. 2022, Article ID 3771752, 19 pages, 2022.

[35] A. S. Veerendra, M. Vasavi Uma maheswari, K. Peddakapu, and C. Punya sekhar, "Enhancement of a grid-connected DFIG wind turbine system using fractional order PI controllers," *Renewable Energy Focus*, vol. 47, Article ID 100506, 2023.

[36] L. Wang and D. N. Truong, "Stability enhancement of DFIG-based offshore wind farm fed to a multi-machine system using a STATCOM," *IEEE Transactions on Power Systems*, vol. 28, no. 3, pp. 2882–2889, 2013.

[37] G. S. Kaloi, J. Wang, and M. H. Baloch, "Active and reactive power control of the doubly fed induction generator based on wind energy conversion system," *Energy Reports*, vol. 2, pp. 194–200, 2016.

[38] P. S. Kundur and O. P. Malik, *Power System Stability and Control*, McGraw-Hill Education, New York, NY, USA, 2022.

[39] S. Kamel, F. Jurado, and Z. Chen, "Power flow control for transmission networks with implicit modeling of static synchronous series compensator," *International Journal of Electrical Power & Energy Systems*, vol. 64, pp. 911–920, 2015.

[40] A. Rashad, S. Kamel, F. Jurado, M. Rihan, and M. Ebeed, "Optimal design of SSSC and crowbar parameters for performance enhancement of Egyptian Zafrana wind farm," *Electrical Engineering*, vol. 104, no. 3, pp. 1441–1457, 2022.

[41] C. A. Ordóñez, A. Gómez-Expósito, and J. M. Maza-Ortega, "Series compensation of transmission systems: a literature survey," *Energies*, vol. 14, no. 6, p. 1717, 2021.

[42] Y. Bai and D. Wang, "Fundamentals of fuzzy logic control-fuzzy sets, fuzzy rules and defuzzifications," in *Advanced Fuzzy Logic Technologies in Industrial Applications*, Y. Bai, H. Zhuang, and D. Wang, Eds., pp. 17–36, Springer London, London, UK, 2006.

[43] A. M. Eltamaly and H. M. Farh, "Maximum power extraction from wind energy system based on fuzzy logic control," *Electric Power Systems Research*, vol. 97, pp. 144–150, 2013.

[44] J. Shi, A. Kalam, and P. Shi, "Improving power quality and stability of wind energy conversion system with fuzzy-controlled STATCOM," *Australian Journal of Electrical and Electronics Engineering*, vol. 12, no. 3, pp. 183–193, 2015.

[45] M. Hemeida, H. Rezk, and M. M. Hamada, "A comprehensive comparison of STATCOM versus SVC-based fuzzy controller for stability improvement of wind farm connected to multi-machine power system," *Electrical Engineering*, vol. 100, no. 2, pp. 935–951, 2018.

[46] J. Ansari, A. R. Abbasi, M. H. Heydari, and Z. Avazzadeh, "Simultaneous design of fuzzy PSS and fuzzy STATCOM controllers for power system stability enhancement," *Alexandria Engineering Journal*, vol. 61, no. 4, pp. 2841–2850, 2022.

[47] K. Khatua and N. Yadav, "Voltage stability enhancement using VSC-OPF including wind farms based on Genetic algorithm," *International Journal of Electrical Power & Energy Systems*, vol. 73, pp. 560–567, 2015.

[48] S. Mokred, Y. Wang, and T. Chen, "Modern voltage stability index for prediction of voltage collapse and estimation of maximum load-ability for weak buses and critical lines identification," *International Journal of Electrical Power & Energy Systems*, vol. 145, Article ID 108596, 2023.

[49] C. Zheng and M. Kezunovic, "Distribution system voltage stability analysis with wind farms integration," in *North American Power Symposium 2010*, pp. 1–6, IEEE, 2010.

[50] E. Vittal, M. O'Malley, and A. Keane, "A steady-state voltage stability analysis of power systems with high penetrations of wind," *IEEE Transactions on Power Systems*, vol. 25, no. 1, pp. 433–442, 2010.

[51] A. Delavari, I. Kamwa, and P. Brunelle, "Simscape power systems benchmarks for education and research in power grid dynamics and control," in *2018 IEEE Canadian Conference on Electrical & Computer Engineering (CCECE)*, pp. 1–5, Quebec City, QC, Canada, August 2018.

[52] K. P. Schneider, B. A. Mather, B. C. Pal et al., "Analytic considerations and design basis for the IEEE distribution test feeders," *IEEE Transactions on Power Systems*, vol. PP, no. 99, pp. 1–1, 2017.

[53] R. Jain, Z. Yingchen, and B. M. Hodge, "Investigating the impact of wind turbines on distribution system stability," in *2016 IEEE Power & Energy Society Innovative Smart Grid Technologies Conference (ISGT)*, pp. 1–5, Quebec City, QC, Canada, January 2016.